GeomechX

User Manual

A Finite Element Code for Thermo-Hydro-Mechanical Coupled Processes in Geomechanics

Version 1.0

Hwajung Yoo

Hyeonkyeong Na

Ki-Bok Min

Department of Energy Systems Engineering

Seoul National University

May 21, 2025

Support email: hwajungyoo@kigam.re.kr (Hwajung Yoo)

1. Table of Contents

Reference Publications

This manual is based on the following academic thesis and journal paper.

For detailed information on the theoretical background, numerical methods, and application examples of GeomechX, please refer to the following:

- Yoo, H. (2025). Development of an Open-source Finite Element Code for Coupled Thermo-Hydro-Mechanical Processes in Geomechanics and Its Application to Deep Borehole Disposal of Radioactive Waste. Ph.D. dissertation, Seoul National University. Korea.

- Yoo, H., & Min, K.-B. (2025). GeomechX: A Finite Element Code for Thermo-Hydro-Mechanical Coupled Processes in Geomechanics, SoftwareX. (in preparation).

If you use GeomechX in your research, please cite the following work:

Yoo, H., & Min, K.-B. (2025). GeomechX: A Finite Element Code for Thermo-Hydro-Mechanical Coupled Processes in Geomechanics, SoftwareX. (in preparation).

License

GeomechX License (LGPL v3)

GeomechX: A Finite Element Code for Thermo-Hydro-Mechanical Coupled Processes in Geomechanics

This program is free software: you can redistribute it and/or modify it under the terms of the GNU Lesser General Public License (LGPL) as published by the Free Software Foundation, either version 3 of the License, or (at your option) any later version.

This program is distributed in the hope that it will be useful, but WITHOUT ANY WARRANTY; without even the implied warranty of MERCHANTABILITY or FITNESS FOR A PARTICULAR PURPOSE. See the GNU Lesser General Public License for more details.

Summary

GeomechX is licensed under the **GNU Lesser General Public License v3.0**.

You are free to:

- Use, modify, and redistribute this software
- Link this software into proprietary applications **via dynamic linking**
- Use it for both academic and commercial purposes

You must:

- **Disclose modifications** to GeomechX itself if distributed
- **Preserve this license notice and attribution**

License Upgrade Notice

The authors reserve the right to relicense future versions of GeomechX under a more permissive license, such as BSD 3-Clause.

Full License Text

The full license text is omitted here for brevity.
For complete terms, see the official GNU Lesser General Public License v3.0: https://www.gnu.org/licenses/lgpl-3.0.html

1. Introduction

GeomechX is a finite element code designed for modeling thermo-hydro-mechanical (THM) coupled processes and single physical processes in geomechanics, applicable to both field- and lab-scale simulations. Developed on a Linux-based Ubuntu operating system, GeomechX is also compatible with WSL2 (Windows Subsystem for Linux 2). Written in C++, the code utilizes object-oriented programming principles, facilitating the development of modular physics components that can be adapted or extended as needed.

2. Code structure

The architecture of GeomechX is organized into key directories, each dedicated to specific components of the THM simulation framework. Figure 2-1 shows the general structure of GeomechX. The Base directory provides essential functions and classes for material property setup and mesh handling. The BoundaryCondition directory includes functions and classes for defining boundary conditions across physics modules; for instance, the BCElasticity class offers boundary options such as free, roller, fixed, displacement, normal stress, and traction conditions. The PointwiseFunctions directory contains pointwise functions used in finite element method (FEM) calculations, providing residual and Jacobian evaluations based on conventions outlined in Knepley et al. (2013). These pointwise functions are essential for the numerical solution of different physics models within the THM framework. The Physics directory houses core functions managing domain settings, parameters, finite elements, boundaries, input parameters, solution fields, and derived fields. This directory leverages classes from the Base, BoundaryCondition, and PointwiseFunctions directories to enable a seamless integration of physics models within the simulation. The Mains directory comprises scripts to initialize and control the simulation process, parse input files, manage workflow, and finalize the program, primarily by invoking functions from the Physics directory in a specified sequence.

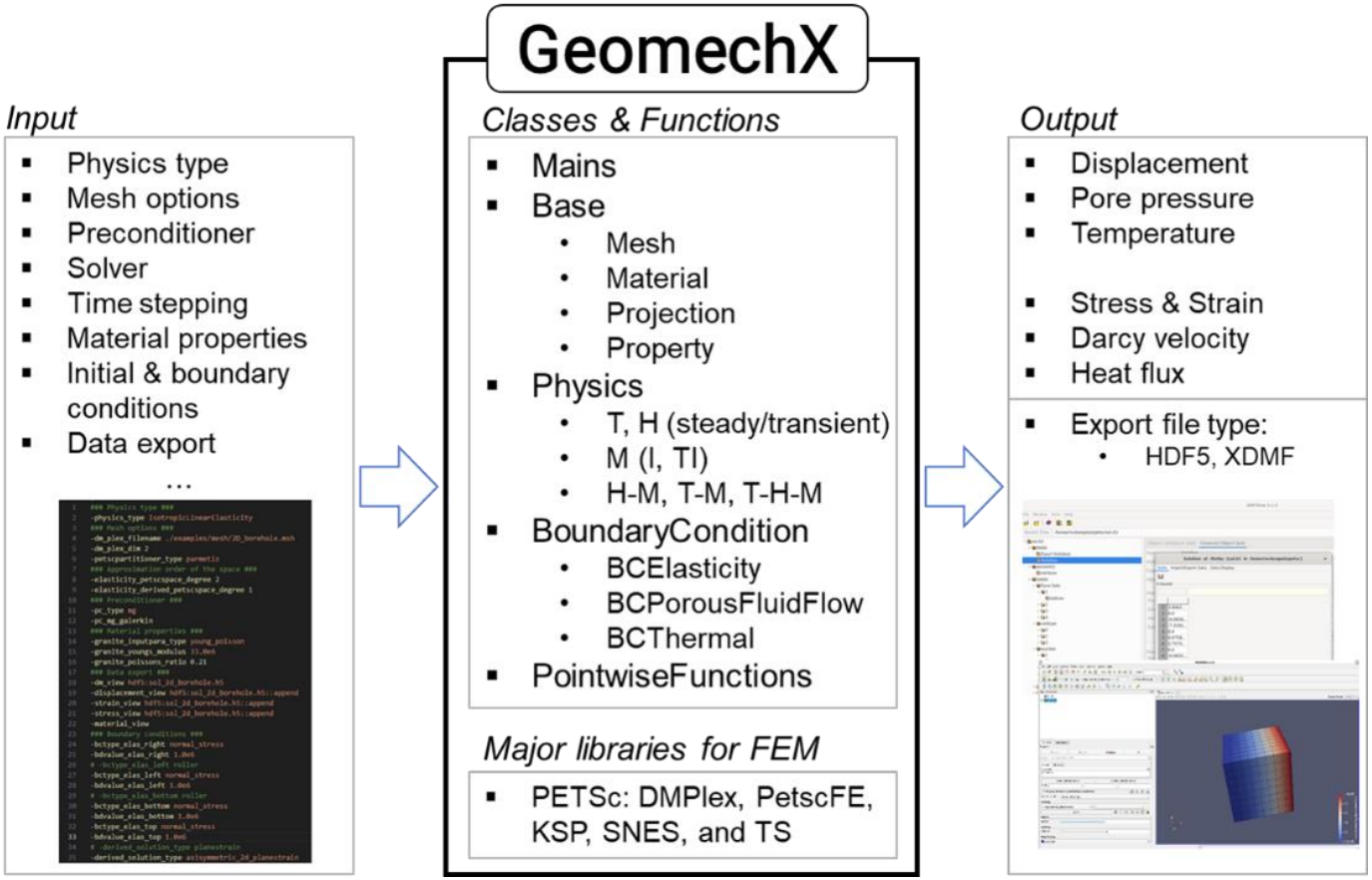

Figure 2-1 Structure of GeomechX and inputs and outputs of the program.

3. Installation & Usage

3.1. Prerequisites & Recommendations

3.1.1 Prerequisites

PETSc (Portable, Extensible Toolkit for Scientific Computation)

PETSc is a core dependency for running GeomechX. The current version of GeomechX has been tested with PETSc version 3.20. To install PETSc, please refer to the official installation guide:

https://petsc.org/release/install/download/

Before installing PETSc, ensure that all prerequisite packages listed in the guide are available on your system.

Key dependencies include:

- BLAS/LAPACK – Required by PETSc
- HDF5, CMake, MuParser, and MPI (MPICH or OpenMPI) – Required by GeomechX
- METIS and ParMETIS – Recommended for mesh partitioning and solver performance

If these libraries are not already installed on your system, PETSc provides configuration options to download and build them automatically.

Example Configuration Command:

```
./configure --with-debugging=0 --with-x=1 --download-triangle --download-ctetgen --download-hdf5 --download-metis --download-parmetis=yes --download-superlu_dist --download-mumps --download-scalapack --download-cmake --with-fc=0 --download-muparser=yes --download-mpich
```

Table 3-1 Description **of Key Configuration Options**

Option	Description
`--with-debugging=0`	Builds PETSc in optimized mode (recommended for performance)
`--with-x=1`	Enables support for X Window System (optional, for

	graphical interfaces)
`--download-triangle`	Downloads Triangle (mesh generation tool) if not already installed (required for some examples)
`--download-ctetgen`	Downloads CTetgen (3D tetrahedral mesh generator) if not already installed (required for some examples)
`--download-hdf5`	Downloads HDF5 for structured data handling (required by GeomechX)
`--download-metis`	Downloads METIS for graph partitioning
`--download-parmetis=yes`	Downloads ParMETIS for parallel partitioning (required by SuperLU_DIST)
`--download-superlu_dist`	Installs SuperLU_DIST external solver
`--download-mumps`	Installs the MUMPS solver (depends on ScaLAPACK)
`--download-scalapack`	Installs ScaLAPACK, required by MUMPS
`--download-cmake`	Downloads CMake build system if not already installed (required by GeomechX)
`--with-fc=0`	Disables Fortran compiler usage (GeomechX does not require Fortran)
`--download-muparser=yes`	Downloads and installs muParser expression parser (required by GeomechX)
`--download-mpich`	Downloads and installs MPICH (alternative: OpenMPI)
`--download-fblaslapack`	Downloads and installs BLAS/LAPACK if not available on your system (required)

3.1.2 Recommendations

For pre- and post-processing, **GeomechX** is compatible with several open-source visualization and mesh generation tools. It is highly recommended to install the following:

- Gmsh: A powerful open-source 3D finite element mesh generator with an integrated CAD engine and post-processor. https://gmsh.info/
- HDFView: A visual tool for browsing and editing HDF5 files. Useful for inspecting input/output data. https://www.hdfgroup.org/download-hdfview/
- ParaView: An open-source application for large-scale data

visualization and post-processing. https://www.paraview.org/

3.2. Installation

3.2.1 Download

The GIT repository for GeomechX is hosted on GitHub. Go to the directory that you want to download the program and run the following commands:

```
git clone https://github.com/yhj0313/GeomechX.git

cd GeomechX
```

3.2.2 Installation

Within the GeomechX directory, execute the following commands to build the program:

```
rm -rf build

mkdir build

cd build

cmake -S ../ -B ./

make all
```

Upon successful compilation, the GeomechX executable file will be located in the build folder.

3.3. Input file

During initialization, GeomechX reads an input configuration file that defines simulation parameters, including physics type, mesh file, solver settings, material properties, boundary conditions, and data export formats.

If a default `.geomechxrc` file is located in the same directory as the executable, it is automatically recognized and loaded as the input file.

3.3.1 Selecting an Input File

Example input files are located in the `examples/input_files` directory. To prepare for a simulation:

1. Select a file corresponding to your modeling scenario.

2. Copy the selected file to your working directory

3. Rename the file to use the `.geomechxrc` extension only, removing any additional descriptors.

3.3.2 Editing the Input File

Once the `.geomechxrc` file is in place, you may adjust the configuration by editing its options and property values as needed:

- All commands must begin with a dash (`-`).

- Each command is typically followed by its corresponding value on the same line.

- Lines beginning with `#` are comments and do not affect the execution.

- Property descriptions are usually listed adjacent to their command.

Defining the Physics Type

To specify the physical model, use the `-physics_type` command. For example:

```
-physics_type IsotropicLinearElasticity
```

The available physics types are listed in Table 3-2.

Table 3-2 Available options for physics types

Options	Description
IsotropicLinearElasticity	Isotropic Linear Elasticity
TransverselyIsotropicLinear Elasticity	Transversely Isotropic Linear Elasticity
SteadyDarcysFlow	Steady hydraulic process in porous media, fully saturated with single-phase, single-component fluid
TransientDarcysFlow	Transient hydraulic process in porous media, fully saturated with single-phase, single-component fluid
SteadyThermal	Steady state thermal process in porous media
TransientThermal	Transient state thermal process in porous media
SteadyThermoElasticity	Steady-state thermo-mechanical coupling with isotropic linear elasticity
TransientThermoElasticity	Transient thermo-mechanical coupling with isotropic linear elasticity
TransientPoroElasticity	Transient hydro-mechanical coupling with isotropic linear elasticity.
TransientThermoPoroElasticity	Thermo-hydro-mechanical coupled model in an ideal, fully saturated porous medium with single-phase fluid.

Mesh Options

Mesh-related options define the geometry and dimension of the simulation:

```
-dm_plex_filename <filename.msh>
-dm_plex_dim <2 or 3>
-petscpartitioner_type <partitioner>
```

Example:

```
-dm_plex_filename ../../examplemesh/2D_borehole_quater.msh
-dm_plex_dim 2
-petscpartitioner_type parmetis
```

Select a mesh appropriate to your simulation (2D or 3D). Set the correct dimension using `-dm_plex_dim`. The `petscpartitioner_type` is typically set to `parmetis`. If changes are required, consult the PETSc documentation for valid partitioner types. GeomechX includes example meshes in ‘examples/mesh/’, but users are free to use custom meshes suited to their needs.

Approximation order of the space

The finite element approximation order for each field can be specified using the following options:

```
-elasticity_petscspace_degree 2

-elasticity_derived_petscspace_degree 1
```

- `elasticity_petscspace_degree`: Sets the approximation degree for the displacement field.

- `elasticity_derived_petscspace_degree`: Sets the approximation degree for derived fields (e.g., strain and stress).

Adjust these values depending on the desired accuracy and computational cost of the simulation. These options are physics-specific.

Preconditioners and solvers

GeomechX leverages PETSc's solver infrastructure. Users can configure solvers and preconditioners by setting PETSc options directly in the input file.

Example configuration using multigrid preconditioning:

```
-pc_type mg

-pc_mg_galerkin
```

- `pc_type`: Defines the type of preconditioner (e.g., `mg` for multigrid, `ilu` for incomplete LU).

- `pc_mg_galerkin`: Enables the Galerkin coarse-grid operator for multigrid.

For a complete list of supported solvers and preconditioners, refer to the PETSc documentation. (Preconditioners; Linear solvers; Non-linear solvers)

Material properties

Material property options are dependent on the selected physics model. For example,

in the case of Isotropic Linear Elasticity, the following commands define the material behavior:

```
### Material properties ###

-granite_inputpara_type young_poisson

-granite_youngs_modulus 33.0e6

-granite_poissons_ratio 0.21
```

- granite_inputpara_type: Specifies the input type for the material model. For isotropic elasticity, young_poisson indicates the use of Young's modulus and Poisson's ratio.
- granite_youngs_modulus: Sets the Young's modulus (in consistent units, e.g., Pa).
- granite_poissons_ratio: Sets the Poisson's ratio.

Please note that input parameters and required properties will vary depending on the chosen physics type. Please refer to Chapter 4 for detailed requirements corresponding to each model.

Data exporting options

To configure data export options in GeomechX, use the following commands in the `.geomechxrc` input file:

```
-dm_view hdf5:<solution file name>
-displacement_view hdf5:<solution file name>::append
-strain_view hdf5:<solution file name>::append
-stress_view hdf5:<solution file name>::append
## Important: Ensure that there are no spaces between the command
and the file name when specifying output files. ##
-material_view
```

Example:

```
-dm_view hdf5:sol_2d_borehole_quarter.h5
-displacement_view hdf5:sol_2d_borehole_quarter.h5::append
-strain_view hdf5:sol_2d_borehole_quarter.h5::append
-stress_view hdf5:sol_2d_borehole_quarter.h5::append
```

```
-material_view
```

Exported solution files are typically saved in a HDF5 format (.h5), compatible with HDFView for numerical data inspection. The `-material_view` command exports material properties and additional user-defined parameters to the output file.

Boundary conditions

Boundary conditions are essential for defining how the model domain interacts with its surroundings. In GeomechX, boundary conditions are specified using -bctype_ and -bdvalue_ options, followed by the boundary location and corresponding values.

Below is an example configuration for applying normal stress on all four boundaries of a 2D domain:

```
### Boundary conditions ###

-bctype_elas_right normal_stress

-bdvalue_elas_right 12.0e6

-bctype_elas_left normal_stress

-bdvalue_elas_left 12.0e6

-bctype_elas_bottom normal_stress

-bdvalue_elas_bottom 8.0e6

-bctype_elas_top normal_stress

-bdvalue_elas_top 8.0e6
```

- bctype_elas_<boundary>: Defines the type of boundary condition for a specific boundary (e.g., normal_stress, displacement, roller, etc.).
- bdvalue_elas_<boundary>: Specifies the magnitude or value of the condition applied.

Note:

- Boundary names typically include right, left, top, and bottom for 2D domains.

- The types of boundary conditions available may depend on the selected physics model.
- Always ensure consistency between boundary condition type and value.

Refer to Chapter 4 for physics-specific boundary condition options and examples.

Naming Convention for Input Files

Use clear and descriptive file names in the `input_files` directory to prevent confusion. For example:

```
#borehole_2d.geomechxrc
```

Refer to Chapter 4 for physics-specific input requirements. Once the input file is configured, save it and name it `.geomechxrc`.

Example input file

```
### Physics type ###

-physics_type IsotropicLinearElasticity

### Mesh options ###

-dm_plex_filename ../../examplemesh/2D_borehole.msh

-dm_plex_dim 2

-petscpartitioner_type parmetis

### Approximation order of the space ###

-elasticity_petscspace_degree 2

-elasticity_derived_petscspace_degree 1

### Preconditioner ###

-pc_type mg

-pc_mg_galerkin

### Material properties ###
```

```
-granite_inputpara_type young_poisson
-granite_youngs_modulus 33.0e6
-granite_poissons_ratio 0.21
### Data export ###
-dm_view hdf5:sol_2d_borehole.h5
-displacement_view hdf5:sol_2d_borehole.h5::append
-strain_view hdf5:sol_2d_borehole.h5::append
-stress_view hdf5:sol_2d_borehole.h5::append
-material_view
### Boundary conditions ###
-bctype_elas_right normal_stress
-bdvalue_elas_right 12.0e6
-bctype_elas_left normal_stress
-bdvalue_elas_left 12.0e6
-bctype_elas_bottom normal_stress
-bdvalue_elas_bottom 8.0e6
-bctype_elas_top normal_stress
-bdvalue_elas_top 8.0e6
# -derived_solution_type planestrain
-derived_solution_type axisymmetric_2d_planestrain
### Name of this file ###
#borehole_2d.geomechxrc
```

3.4. Execution

To execute a simulation using GeomechX, ensure that both the executable file (`GeomechX`) and the input configuration file (`.geomechxrc`) are located in the same working directory.

3.4.1 Running in Serial Mode

To run the simulation in serial (single-threaded) mode, navigate to your working directory and enter the following command:

```
./GeomechX
```

3.4.2 Running in Parallel Mode

To run the simulation in parallel using MPI (Message Passing Interface), use the following command:

```
mpiexec -n <number_of_processes> ./GeomechX
```

- Replace `<number_of_processes>` with the number of MPI processes (threads) you wish to use.

- Ensure that MPI (e.g., MPICH or OpenMPI) is correctly installed and configured on your system.

Note: When running in parallel, the number of processes should match the number of available cores.

3.5. Export and Visualization

Simulation results are exported to an HDF5 (.h5) file as specified in the input configuration file (.geomechxrc). These files contain field data such as displacement, stress, and strain.

Generating XDMF Files

To visualize the results in ParaView, the .h5 data must first be linked with an .xdmf file. This can be done using the provided Python script:

```
/your_geomechx_location/examples/geomechx_xdmf/petsc_gen_xdmf_2_radial.py sol_2d_borehole_quarter.h
```

- Replace `/your_geomechx_location/` with the path to your local GeomechX installation.

- Replace `sol_2d_borehole_quarter.h5` with the name of your HDF5 output file.

File Format Overview

GeomechX supports two primary file formats for output:

Table 3-3 Primary file formats for output

Format	Purpose
.h5	HDF5 format for structured data. Compatible with HDFView for data inspection and debugging.
.xdmf	XDMF (XML) format used for visualization. Compatible with ParaView for post-processing and rendering.

Tip: Always generate the `.xdmf` file after simulation if you intend to use ParaView for visualizing results.

4. Physics models

4.1. Isotropic Linear Elasticity

4.1.1 Governing equation

The linear elasticity model has a variable field of displacement. GeomechX provides two options for linear elasticity, isotropic and transversely isotropic elasticity modules. The linear elasticity solves the mechanical equilibrium equations (Jaeger et al., 2007):

$$-\nabla \cdot \sigma = f \tag{4-1}$$

where σ is the stress tensor, and f is the body force. In linear isotropic elasticity, the stress-strain law, often called “Hooke’s law,” is written as

$$\sigma = \lambda I trace(\varepsilon) + 2\mu\varepsilon \tag{4-2}$$

where λ is Lame’s first parameter, μ is the shear modulus, and ε is the strain tensor, which is expressed as

$$\varepsilon = \frac{1}{2}(\nabla u + (\nabla u)^T) \tag{4-3}$$

where u is the displacement. Combining Eqs. (4-2) and (4-3) and substituting the stress tensor in Eq. (4-1), we obtain the displacement form of the equilibrium equations:

$$(\lambda + \mu)\nabla(\nabla \cdot u) + \mu\nabla^2 u + f = 0, \tag{4-4}$$

which is known as the Navier equations. The linear elasticity module solves the displacement fields using Eq. (4-4)

4.1.2 Input file

To configure simulations for isotropic linear elasticity, you may refer to example input files located in:

`/examples/input_files/Elasticity/IsotropicLinearElasticity`

These example `.geomechxrc` files provide templates for configuring key simulation parameters.

Specifying the Approximation Order

```
-elasticity_petscspace_degree <space degree>
-elasticity_derived_petscspace_degree <space degree for derived fields>
```

Example

```
-elasticity_petscspace_degree 2
-elasticity_derived_petscspace_degree 1
```

The first option '`-elasticity_petscspace_degree`' specifies the polynomial degree for the displacement field (0 to 4). Values of 1 or 2 are generally sufficient for accurate results. The second option '`-elasticity_derived_petscspace_degree`' sets the degree for stress and strain, which are spatial derivatives of displacement. Testing has shown that settings of 2 for displacement and 1 for stress and strain are often appropriate and computationally efficient.

Specifying Material Properties

```
-granite_inputpara_type <parameter type>
-granite_youngs_modulus <value>
```

```
-granite_poissons_ratio <value>
-granite_lames_first_parameter <value>
-granite_shear_modulus <value>
-granite_bulk_modulus <value>
```

Example:

```
-granite_inputpara_type young_poisson
-granite_youngs_modulus 33.0e9
-granite_poissons_ratio 0.21
```

Table 4-1 Supported input types for material property

Option	Description
young_poisson	Young's modulus and Poisson's ratio
young_shear	Young's modulus and shear modulus
bulk_shear	Bulk modulus and shear modulus
lames	Lame's 1st and 2nd constants (λ and μ)

Specify one of the above types along with its two associated parameters. GeomechX will compute the others. If no type is specified, the system defaults to `lames` with both constants set to 1.0.

Defining Boundary Conditions

Boundary conditions must be specified for all boundaries of the domain. Boundary options for 2D are 'left', 'right', 'top', and 'bottom'. For 3D meshes, include `front` and `back`. When using `normal_stress`, provide a scalar. For `displacement` or `traction`, include vector components for x, y, and z directions.

Entering boundary conditions

```
-bctype_elas_<boundary> <condition type>
-bdvalue_elas_<boundary> <value>
```

Example:

```
-bctype_elas_right normal_stress
-bdvalue_elas_right 12.0e6
-bctype_elas_left roller
```

```
-bctype_elas_bottom roller
-bctype_elas_top normal_stress
-bdvalue_elas_top 10.0e6
```

Table 4-**3** Available boundary condition options

Option	Description
free	No constraint
roller	Movement constrained to one axis
fixed	Fully constrained (zero movement)
displacement	Prescribed displacement
normal_stress	Applied stress normal to surface
traction	Applied traction vector

Specifying the Derived Solution Type

Choose an appropriate coordinate system for your model. This setting affects how stress and strain are interpreted during post-processing.

```
-derived_solution_type <coordinate system>
```

Example:

```
-derived_solution_type axisymmetric_2d_planestrain
```

Table 4-**4** Available coordinate system options for derived fields

Option	Description
planestrain	2D orthogonal coordinate system
axisymmetric_2d_planestrain	2D polar coordinate system
cauchy_3d	3D orthogonal coordinate system
axisymmetric_3d	3D cylindrical coordinate system

4.1.3 Output

Isotropic Linear Elasticity include both solution fields and derived fields:

Solution fields:

- Displacement fields

Derived fields:

- Stress tensor components

- Strain tensor components

Outputs are written to the `.h5` file specified in the input file. See Chapter 3.5 for more details.

4.1.4 Verification

Refer to Chapter 5.1 for verification examples and benchmark cases related to isotropic linear elasticity.

4.2. Transversely isotropic linear elasticity

4.2.1 Governing equation

Transversely isotropic rock exhibits a unique symmetry where one of the three Cartesian coordinate axes serves as an axis of rotational symmetry. This implies that all directions perpendicular to this axis are elastically equivalent, and the elastic material behaves isotropically within any plane normal to this axis. In the transversely isotropic elasticity module, the y-axis is defined as the axis of rotational symmetry, resulting in xz-planes of isotropy.

Five independent elastic constants characterize the mechanical behavior of such rocks: elastic moduli (E_1 and E_2), shear modulus (G_2), and Poisson's ratios (ν_1 and ν_2). These constants are defined as $E_1 = E_x = E_z$, $E_2 = E_y$, $G_2 = G_{yz} = G_{xy}$, $\nu_1 = \nu_{xz}$, and $\nu_2 = \nu_{yx} = \nu_{yz}$ (Cho et al., 2012). The constitutive relationship for transversely isotropic rock is expressed as:

$$\begin{bmatrix} \varepsilon_x \\ \varepsilon_y \\ \varepsilon_z \\ \gamma_{yz} \\ \gamma_{zx} \\ \gamma_{xy} \end{bmatrix} = \begin{bmatrix} \frac{1}{E_1} & -\frac{\nu_2}{E_2} & -\frac{\nu_1}{E_1} & 0 & 0 & 0 \\ -\frac{\nu_2}{E_2} & \frac{1}{E_2} & -\frac{\nu_2}{E_2} & 0 & 0 & 0 \\ -\frac{\nu_1}{E_1} & -\frac{\nu_2}{E_2} & \frac{1}{E_1} & 0 & 0 & 0 \\ 0 & 0 & 0 & \frac{1}{G_2} & 0 & 0 \\ 0 & 0 & 0 & 0 & \frac{2(1+\nu_1)}{E_1} & 0 \\ 0 & 0 & 0 & 0 & 0 & \frac{1}{G_2} \end{bmatrix} \begin{bmatrix} \sigma_x \\ \sigma_y \\ \sigma_z \\ \tau_{yz} \\ \tau_{zx} \\ \tau_{xy} \end{bmatrix} \quad (4\text{-}5)$$

The transversely isotropic elasticity model employs Eq. (4-5) for the stress-strain relationship, superseding the general isotropic formulation given in Eq. (4-2).

4.2.2 Input file

To configure simulations for transversely isotropic linear elasticity, you may refer to example input files located in:

/examples/input_files/Elasticity/TransverselyIsotropicLinearElasticity

These example `.geomechxrc` files provide templates for configuring key simulation parameters.

The following configuration options are identical to those used for Isotropic Linear Elasticity (Chapter 4.1):

- Specifying the Approximation Order,
- Defining Boundary Conditions and,
- Specifying the Derived Solution Type

Specifying Material Properties

In the transversely isotropic model, users provide five elasticity constants using following commands in the .geomechxrc file:

```
-granite_inputpara_type fiveparameters
-granite_youngs_modulus <value for E>
-granite_youngs_modulus_ <value for E'>
-granite_poissons_ratio  <value for ν>
-granite_poissons_ratio_  <value for ν'>
-granite_shear_modulus_  <value for G>
-granite_theta <value for θ>
```

Example:

```
-granite_inputpara_type fiveparameters
-granite_youngs_modulus 60.0e9
-granite_youngs_modulus_ 40.0e9
-granite_poissons_ratio 0.25
-granite_poissons_ratio_ 0.20
-granite_shear_modulus_ 20.0e9
-granite_theta 90
```

Table 4-2 Description of Parameters

Parameter options	Description
-granite_inputpara_type	Must be set to fiveparameters for transversely

	isotropic materials
-granite_youngs_modulus	Young's modulus in the isotropic plane (E)
-granite_youngs_modulus_	Young's modulus in the transverse direction (E′)
-granite_poissons_ratio	Poisson's ratio in the isotropic plane (v)
-granite_poissons_ratio_	Poisson's ratio involving transverse direction (v′)
-granite_shear_modulus_	Shear modulus associated with the transverse direction (G)
-granite_theta	Orientation angle (θ) of the transverse isotropy axis (in degrees)

Note: The underscore (_) suffix in parameters denotes values related to the transverse direction.

4.2.3 Output

Simulation outputs for Transversely Isotropic Linear Elasticity include both solution fields and derived fields:

Solution fields:

- Displacement fields

Derived fields:

- Stress tensor components

- Strain tensor components

Outputs are written to the `.h5` file specified in the input file. For export and visualization guidance, refer to Chapter 3.5

4.2.4 Verification

Refer to Chapter 5.2 for verification examples and benchmark cases related to isotropic linear elasticity.

4.3. Thermal process in porous media

4.3.1 Governing equation

For heat transfer, GeomechX accounts for both conduction and convection (if Darcy velocity q is specified). The governing equation for transient heat transfer is:

$$\rho_r c_{p,r} \frac{\partial T}{\partial t} + \rho_f c_{p,f} q \cdot \nabla T - \nabla \cdot \left(k_{eq} \nabla T\right) = q_T{}''' \tag{4-6}$$

where ρ_r is rock density, $c_{p,r}$ and $c_{p,f}$ are rock and fluid heat capacities, k_{eq} is equivalent thermal conductivity, and $q_T{}'''$ is the heat rate per unit volume. In steady-state models, the first term, $\rho_r c_{p,r} \frac{\partial T}{\partial t}$, in this equation is omitted.

4.3.2 Input file

To configure simulations for thermal processes, you may refer to example input files located in:

`/examples/input_files/Thermal`

These example `.geomechxrc` files provide templates for configuring key simulation parameters.

4.3.3 Output

Simulation outputs for the hydraulic processes include both solution fields and derived fields:

Solution fields:

- Temperature fields

Derived fields:

- Heat flux components

Outputs are written to the `.h5` file specified in the input file. For export and visualization guidance, refer to Chapter 3.5

4.3.4 Verification

Refer to Chapter 5.3 for verification examples and benchmark cases related to thermal processes.

4.4. Hydraulic process in porous media

4.4.1 Governing equation

Darcy's flow and fluid storage in porous media is modeled assuming the porous rock material is fully saturated with single-phase, single-component fluid. Pore pressure (P_p) was set to be the variable in the hydraulic process of porous media. Assuming a rigid and undeformable rock, the transient state was solved by the below equation

$$\phi C \frac{\partial P_p}{\partial t} + \nabla \cdot q = 0 \tag{4-7}$$

where ϕ is porosity, C is fluid compressibility, and pore pressure and Darcy velocity (q) are related as

$$q = -\frac{k}{\mu} \nabla \left(P_p - \rho_f g \cdot x \right) \tag{4-8}$$

where k is permeability, μ is fluid viscosity, ρ_f is fluid density and g is gravitational acceleration, and x represents spatial coordinates. Inserting Eq. (4-8) into Eq. (4-7), the transient Darcy's flow module solves the pore pressure fields of the following equation:

$$\phi C \frac{\partial P_p}{\partial t} - \frac{k}{\mu} (\nabla \cdot \nabla) \left(P_p - \rho_f g \cdot x \right) = 0 \tag{4-9}$$

A steady state problem ignored the time derivative term, $\phi C \frac{\partial P_p}{\partial t}$, in Eq. (4-7).

4.4.2 Input file

To configure simulations for transversely isotropic linear elasticity, you may refer to example input files located in:

`/examples/input_files/PorousFluidFlow`

These example `.geomechxrc` files provide templates for configuring key

simulation parameters.

4.4.3 Output

Simulation outputs for the hydraulic processes include both solution fields and derived fields:

Solution fields:

- Pore pressure fields

Derived fields:

- Darcy's velocity components

Outputs are written to the `.h5` file specified in the input file. For export and visualization guidance, refer to Chapter 3.5

4.4.4 Verification

Refer to Chapter 5.4 for verification examples and benchmark cases related to hydraulic processes.

4.5. Thermo-mechanical coupled model

4.5.1 Governing equation

For the thermo-mechanical process, the temperature field is coupled with isotropic linear elasticity through the displacement field. Considering the thermal stress generated due to temperature changes, the stress-strain relation in Eq. (4-2) is modified as:

$$\sigma = \lambda I trace(\varepsilon) + 2\mu\varepsilon - 3\beta K(T - T_{ref}) \tag{4-10}$$

where β is the linear thermal expansion coefficient, K is the bulk modulus, and T_{ref} is the reference temperature for thermal stress calculations. The mechanical equilibrium equation, Eq. (4-1), is written using Eqs. (4-3) and (4-10):

$$(\lambda + \mu)\nabla(\nabla \cdot u) + \mu\nabla^2 u + f - 3\beta K\nabla T = 0, \tag{4-11}$$

In the thermo-mechanical diffusion equation for temperature, the thermal coupling is considered weak because the effect of mechanical deformation on the temperature is generally negligible. According to McTigue (1986), the thermo-mechanical diffusion equation can be reduced to Eq. (4-6) if following condition is satisfied,

$$\frac{9K\beta^2 T_0}{\rho c_v} \ll 1 \tag{4-12}$$

where c_v is the specific heat at constant strain, and T_0 is the reference temperature. Consequently, GeomechX neglects the thermal coupling in the diffusion equation, and solves Eq. (4-6).

4.5.2 Input file

To configure simulations for thermo-mechanical processes, you may refer to example input files located in:

`/examples/input_files/ThermoElasticity`

These example `.geomechxrc` files provide templates for configuring key simulation parameters.

4.5.3 Output

Simulation outputs for the thermo-mechanical processes include both solution fields and derived fields:

Solution fields:

- Temperature fields

- Displacement fields

Derived fields:

- Heat flux components

- Stress tensor components

- Strain tensor components

Outputs are written to the `.h5` file specified in the input file. For export and visualization guidance, refer to Chapter 3.5

4.5.4 Verification

Refer to Chapter 5.5 for verification examples and benchmark cases related to thermo-mechanical processes.

4.6. Hydro-mechanical coupled model

4.6.1 Governing equation

In hydro-mechanical coupled processes, Eq. (4-2) was converted to Eq. (4-13) in consideration of effective stress.

$$\sigma = \lambda I trace(\varepsilon) + 2\mu\varepsilon - \alpha P_p \tag{4-13}$$

where α is Biot coefficient. The poroelastic version of the Navier equation for displacement is derived as:

$$(\lambda + \mu)\nabla(\nabla \cdot u) + \mu\nabla^2 u + f - \alpha\nabla P_p = 0, \tag{4-14}$$

In transient problems, Eq. (4-7) was substituted to

$$\frac{1}{M}\frac{\partial P_p}{\partial t} + \alpha\frac{\partial \varepsilon_b}{\partial t} + \nabla \cdot q = 0 \tag{4-15}$$

where M is Biot Modulus and ε_b is volumetric strain. The volumetric strain was considered as an additional variable field using the following equation,

$$trace\left(\frac{1}{2}(\nabla u + (\nabla u)^T)\right) - \varepsilon_b = 0\ , \tag{4-16}$$

making a mixed formulation for stability, as included in Walker et al. (2023).

4.6.2 Input file

To configure simulations for hydro-mechanical processes, you may refer to example input files located in:

`/examples/input_files/PoroElasticity`

These example `.geomechxrc` files provide templates for configuring key simulation parameters.

4.6.3 Output

Simulation outputs for the hydro-mechanical processes include both solution fields and derived fields:

Solution fields:

- Pore pressure fields

- Displacement fields

Derived fields:

- Darcy's flow components

- Stress tensor components

- Strain tensor components

Outputs are written to the `.h5` file specified in the input file. For export and visualization guidance, refer to Chapter 3.5

4.6.4 Verification

Refer to Chapter 5.6 for verification examples and benchmark cases related to hydro-mechanical processes.

4.7. Thermo-hydro-mechanical coupled model

4.7.1 Governing equation

In the coupled THM simulations, GeomechX models an ideal, fully saturated porous medium with single-phase fluid. In the thermoporoelasticity module, the software couples isotropic linear elasticity (displacement field, u) with temperature (T) and pore pressure (P_p) fields. The primary governing equations are Eqs. (4-1) and (4-3), and following equation:

$$\sigma = \lambda Itrace(\varepsilon) + 2\mu\varepsilon - \alpha P_p - K\beta_d(T - T_{ref}) \tag{4-17}$$

where β_{d} is the drained coefficient of volumetric thermal expansion for porous medium frame. Eq. (4-17) takes into account thermal stress and effective stress. The displacement form of the equilibrium equations in thermoporoelasticity is expressed as:

$$(\lambda + \mu)\nabla(\nabla \cdot u) + \mu\nabla^2 u + f - \alpha\nabla P_p - K\beta_d\nabla T = 0, \tag{4-18}$$

The temperature field is calculated by Eq. (4-6). The pore pressure diffusion equation is

$$\frac{1}{M}\frac{\partial P_p}{\partial t} + \alpha\frac{\partial \varepsilon_b}{\partial t} - \beta_e\frac{\partial T}{\partial t} + \nabla \cdot q = 0 \tag{4-19}$$

where β_e is the volumetric thermal expansion coefficient for fluid content. For ideal porous media with constant porosity (ϕ), the thermal expansion coefficients relate as:

$$\beta_e = \alpha\beta_s + \phi(\beta_f - \beta_s) \tag{4-20}$$

where β_s (approximately equal to β_d) and β_f are the coefficients of volumetric thermal expansion for solid and fluid, respectively. The volumetric strain was also

considered as an additional variable field using Eq (4-16).

4.7.2 Input file

To configure simulations for thermo-hydro-mechanical processes, you may refer to example input files located in:

```
/examples/input_files/ThermoPoroElasticity
```

These example `.geomechxrc` files provide templates for configuring key simulation parameters.

4.7.3 Output

Simulation outputs for the thermo-hydro-mechanical processes include both solution fields and derived fields:

Solution fields:

- Pore pressure fields
- Temperature fields
- Displacement fields

Derived fields:

- Darcy's flow components
- Heat flux components
- Stress tensor components
- Strain tensor components

Outputs are written to the `.h5` file specified in the input file. For export and visualization guidance, refer to Chapter 3.5

4.7.4 Verification

Refer to Chapter 5.7 for verification examples and benchmark cases related to thermo-hydro-mechanical processes.

5. Example problems

The following example problems are drawn from the doctoral dissertation listed below. They demonstrate the application of GeomechX to various geomechanical scenarios, including coupled thermo-hydro-mechanical processes.

Reference:

Yoo, H. (2025). Development of an Open-source Finite Element Code for Coupled Thermo-Hydro-Mechanical Processes in Geomechanics and Its Application to Deep Borehole Disposal of Radioactive Waste (Ph.D. dissertation). Seoul National University, Korea.

These examples serve both as verification cases and practical templates for building user-defined models.

5.1. Isotropic linear elasticity

To verify the isotropic linear elasticity model, numerical simulations were conducted benchmarked against the Kirsch solution (Kirsch, 1898). The Kirsch solution is a well-established analytical framework for predicting elastic stress distribution around a circular opening, such as tunnels and boreholes (**오류! 참조 원본을 찾을 수 없습니다.**). It assumes that the rock mass is elastic, uniform, and isotropic, with a uniform initial stress field. The stress components in two dimensions are defined as follows (Jaeger et al., 2007):

$$\sigma_r = \frac{(\sigma_{Hmax} + \sigma_{hmin})}{2}\left(1 - \frac{R^2}{r^2}\right) + \frac{(\sigma_{Hmax} - \sigma_{hmin})}{2}\left(1 - \frac{4R^2}{r^2} + \frac{3R^4}{r^4}\right)\cos 2\theta \tag{5-1}$$

$$\sigma_\theta = \frac{(\sigma_{Hmax} + \sigma_{hmin})}{2}\left(1 + \frac{R^2}{r^2}\right) - \frac{(\sigma_{Hmax} - \sigma_{hmin})}{2}\left(1 + \frac{3R^4}{r^4}\right)\cos 2\theta \quad (5\text{-}2)$$

$$\tau_{r\theta} = -\frac{(\sigma_{Hmax} - \sigma_{hmin})}{2}\left(1 + \frac{2R^2}{r^2} - \frac{3R^4}{r^4}\right)\sin 2\theta \quad (5\text{-}3)$$

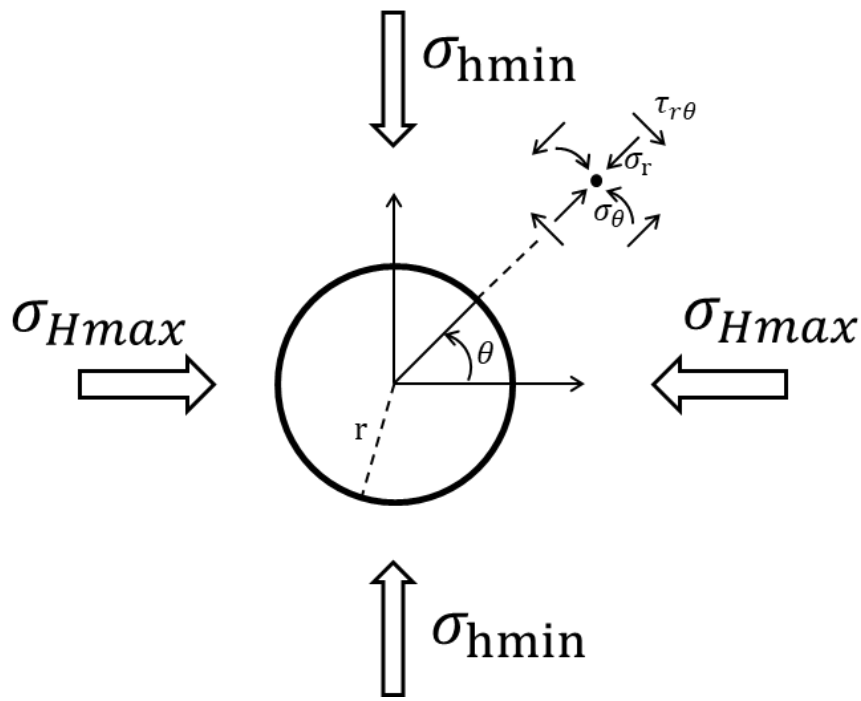

Figure 5-1 Schematic of the Kirsch solution.

A two-dimensional quarter model and a full two-dimensional model were developed (Figure 5-2a and b). For both models, the maximum principal compressive stress of 12 MPa was applied in the x-direction, and the minimum principal compressive stress of 8 MPa was in applied the y-direction. The elastic constants, geometry information, and boundary conditions are summarized in

Table 5-1. Radial and tangential stress were monitored along lines OA and OB, which were shown Figure 5-2c.

Figure 5-3 compares the radial and tangential stress distributions from the numerical simulations with the analytical solutions. Both the quarter and full models showed excellent agreement with the analytical results, confirming the accuracy of the numerical model.

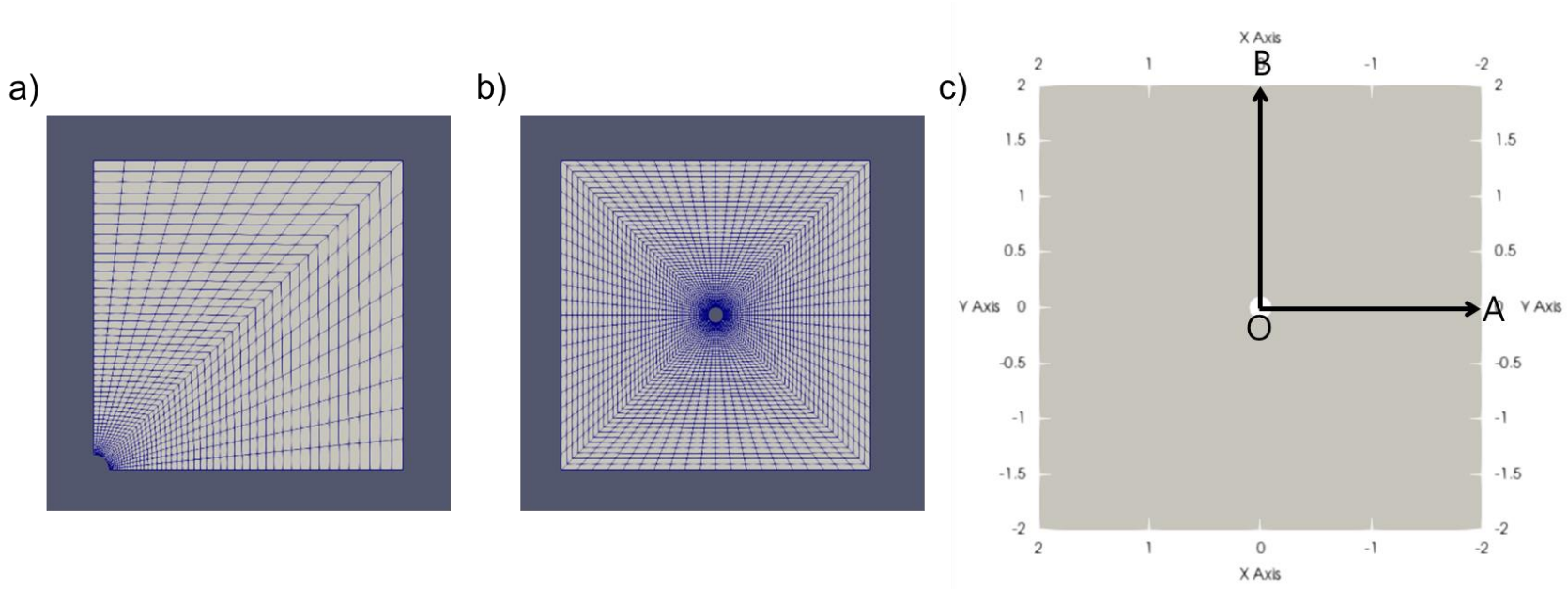

Figure 5-2 (a-b) Model geometry of (a) the two-dimensional quarter model and (b) a full two-dimensional model. (c) Monitoring lines OA and OB of the results.

Table 5-1 Model setup for the verification study of the Kirsch solution.

		2D ¼ model	**2D model**
		Plane strain	
Geometry	Model size (m)	2 × 2	4 × 4
	Borehole radius (m)	0.1	
	Number of elements	1,000	4,000
Stress condition	σ_{Hmax} (MPa)	12	
	$\sigma_{\mathrm{h}min}$ (MPa)	8	
Boundary condition	Roller boundary	x=0 and y=0	-
	Stress boundary	x=2 and y=2	x=2, x=-2, y=2, and y=-2
	Free boundary	r=0.1	r=0.1
Material property	Young's modulus (GPa)	33.0	
	Poisson's ratio	0.21	

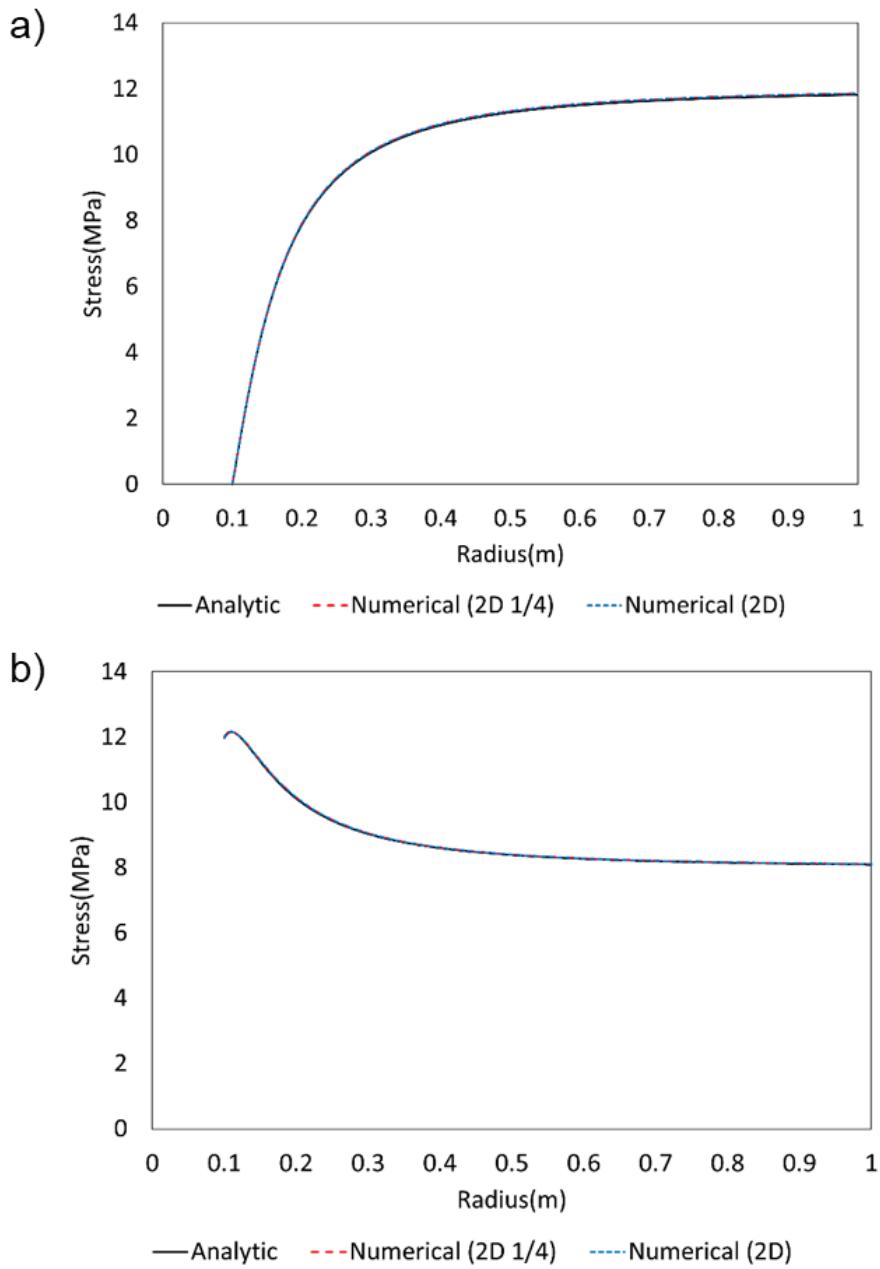

Figure 5-3 Comparison between the analytic solution and results derived from the 2D quarter and full models: (a) Radial stress following line OA, (b) Tangential stress following line OA, (c) Radial stress following line OB, (d) Tangential stress following line OB.

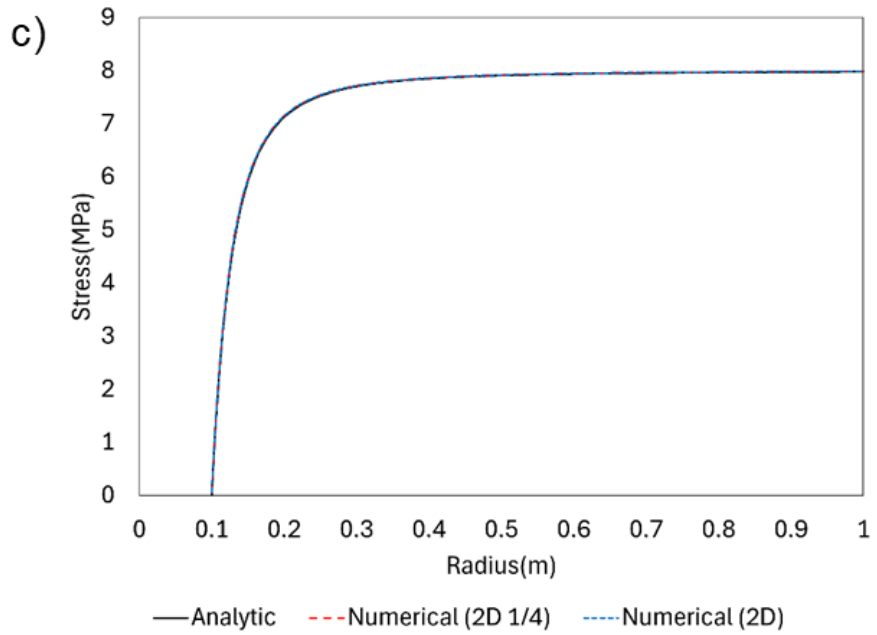

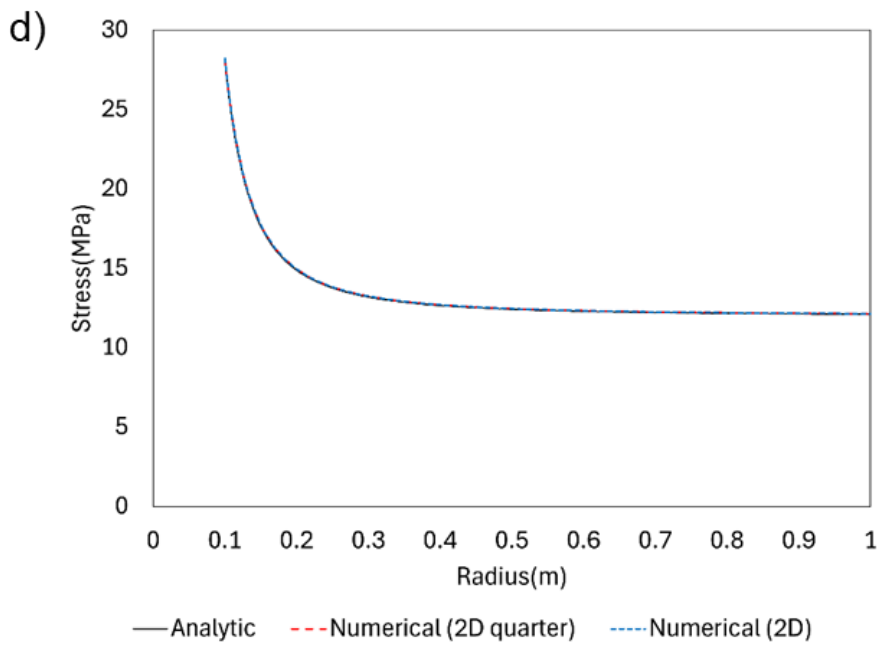

Figure 5-3 Comparison between the analytic solution and results derived from the 2D quarter and full models: (a) Radial stress following line OA, (b) Tangential stress following line OA, (c) Radial stress following line OB, (d) Tangential stress following line OB.

5.2. Transversely isotropic linear elasticity

A uniaxial stress was applied to a three-dimensional cubic sample while varying the inclination angles of the isotropic plane (Figure 5-4). A vertical normal stress of 1 MPa was applied to the top boundary, with a roller boundary condition imposed on the bottom boundary. The lateral boundaries were left free to move. The five elastic constants used in this model are presented in Table 5-2. To verify the results, the same problem was also modeled using a commercial finite element code, COMSOL Multiphysics (COMSOL, 2007), for comparison. The analytical solutions for strains are

$$\varepsilon'_{xx} = \sigma'_{yy}[\frac{sin^2\,2\theta}{4}\left(\frac{1}{E_1}+\frac{1}{E_2}-\frac{1}{G_2}\right)-\frac{\nu_2}{E_2}(cos^4\,\theta+sin^4\,\theta)] \tag{5-4}$$

$$\varepsilon'_{yy} = \sigma'_{yy}[\frac{sin^4\,\theta}{E_1}+\frac{cos^4\,\theta}{E_2}+\frac{sin^2\,2\theta}{4}\left(-\frac{2\nu_2}{E_2}+\frac{1}{G_2}\right)] \tag{5-5}$$

$$\varepsilon'_{zz} = \sigma'_{yy}(-sin^2\,\theta\frac{\nu_1}{E_1}-cos^2\,\theta\frac{\nu_2}{E_2}) \tag{5-6}$$

where θ is the inclination angle of the isotropic plane.

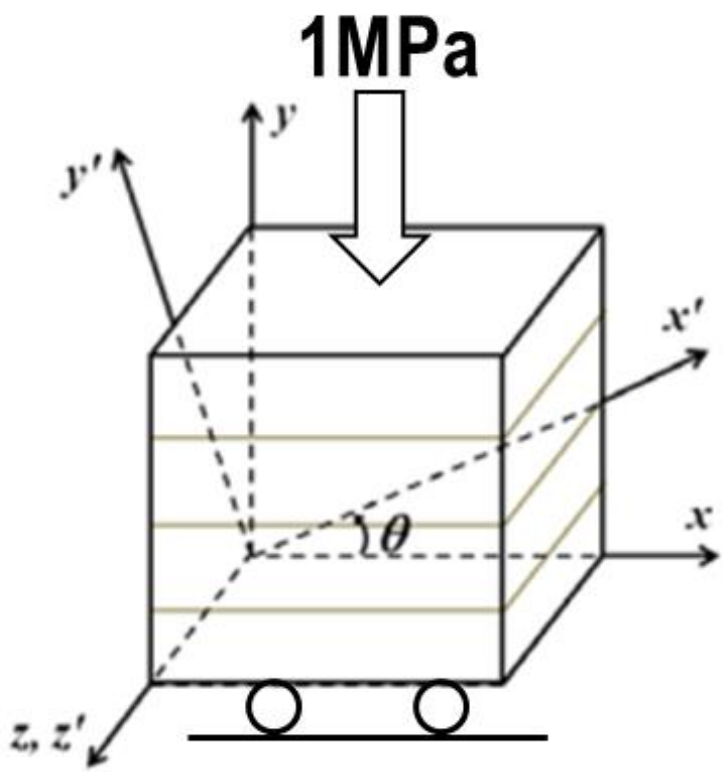

Figure 5-4 Schematic diagram of the verification model of the transversely isotropic elasticity module.

Table 5-2 Input parameters for the verification model of the transversely isotropic elasticity module.

Properties	Values
Young's modulus, E_1	60 GPa
Young's modulus, E_2	40 GPa
Poisson's ratio, ν_1	0.25
Poisson's ratio, ν_2	0.20
Shear modulus, G_2	20 GPa
Inclination angles of isotropic plane, θ	0, 15, 30, 45, 60, 75, and 90 °
Model size	1 m × 1 m × 1 m

Figure 5-5 illustrates the comparison of strain components across different inclination angles. The strain results from GeomechX matched the analytical solutions and the results obtained from the commercial software. Notably, the shear strain, ε'_{xy}, was accurately generated, which highlights the characteristics of the transversely isotropic material. This example confirms the capability of the transversely isotropic elasticity module in GeomechX.

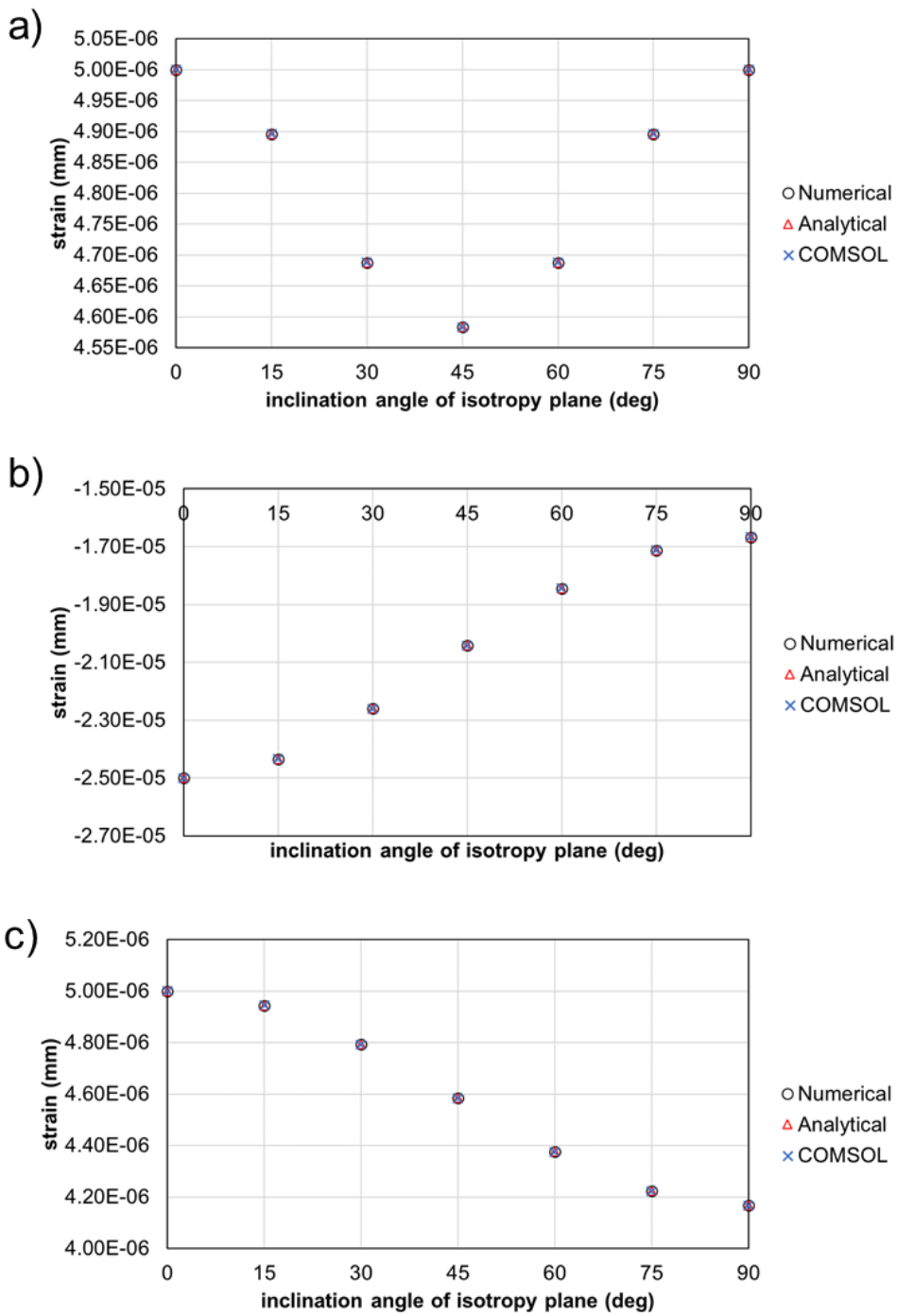

Figure 5-5 Strain comparison across different inclination angles: a) ε'_{xx}, b) ε'_{yy}, c) ε'_{zz}, d) ε'_{xy}.

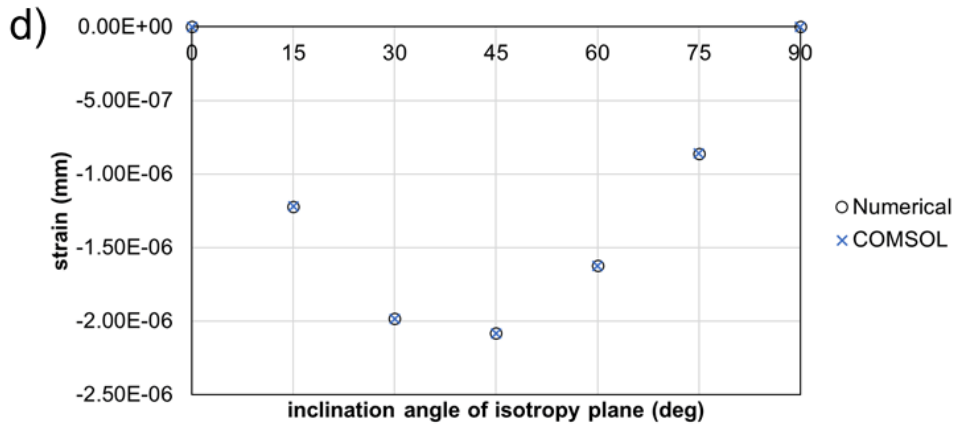

Figure 5-5 Strain comparison across different inclination angles: a) ε'_{xx}, b) ε'_{yy}, c) ε'_{zz}, d) ε'_{xy}.

5.3. Thermal process

5.3.1 Steady conduction-convection heat transfer

The conduction-convection heat transfer at steady state was verified by modeling a constant one-dimensional fluid velocity, u, with boundary constant temperature of T0 and T1 at each side (Figure 5-6). The Peclet number ($\mathrm{N_{PE}}$) of the system (Bergman, 2011) is written as

$$N_{PE} = \rho_f c_{p,f} L / k_{eq} \tag{5-7}$$

where ρ_f is fluid density, $c_{p,f}$ is fluid heat capacity, L is the length of the system, and k_{eq} is equivalent thermal conductivity. The temperature is expressed as

$$T(x) = T_0 + (T_1 - T_0)\frac{\left\{exp\left(\frac{N_{PE}x}{L}\right) - 1\right\}}{\{exp(N_{PE}) - 1\}} \tag{5-8}$$

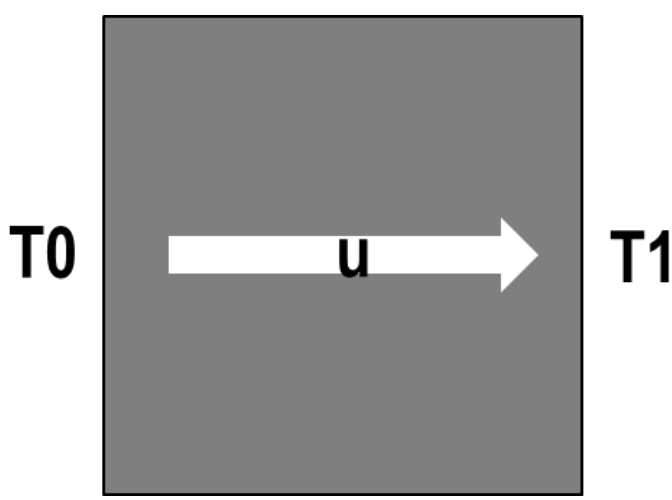

Figure 5-6 Schematic of the steady conduction-convection heat transfer

model.

To verify the steady heat transfer model, a two-dimensional model was constructed sized 1 m × 1 m with 578 triangular elements (Figure 5-7). Boundary temperatures were $T_0 = 20℃$ and $T_1 = 60℃$, and material properties were set to be $\rho_f = 1{,}000\ \mathrm{kg/m^3}$, $c_{p,f} = 4{,}182$ J/kg K, and $k_{eq} = 3.5$ W/m K. Seven different fluid velocity were tested, which corresponded to seven Peclet numbers as presented in Table 5-3.

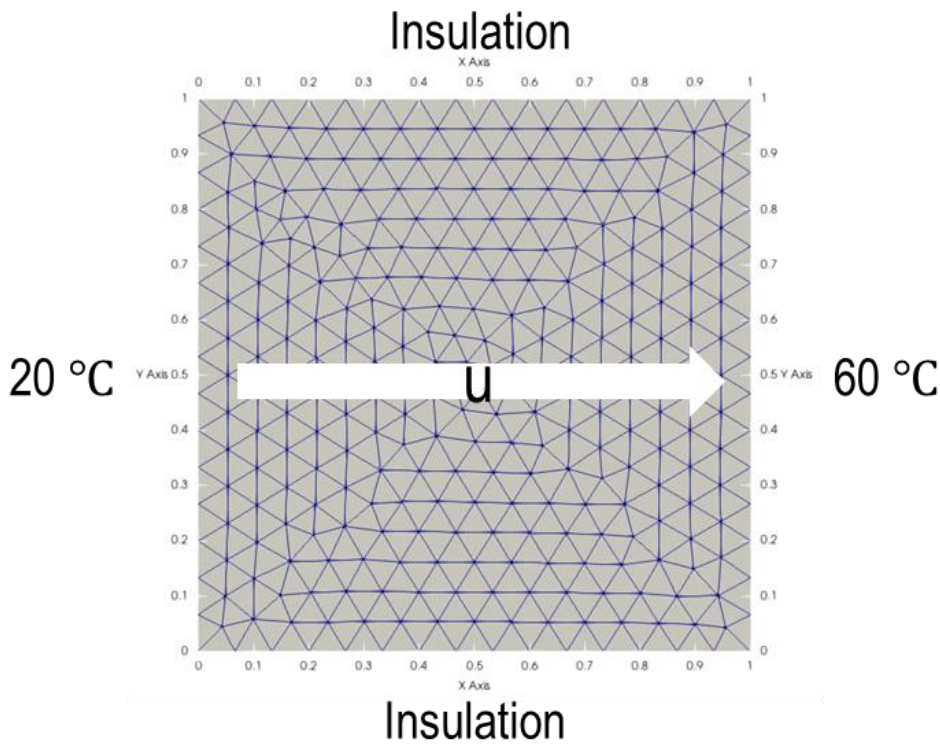

Figure 5-7 Model setup for the steady conduction-convection heat transfer model.

Table 5-3 Peclet numbers and fluid velocities for seven simulation cases.

Simulation cases	Peclet number (N_{PE})	Fluid velocity [m/s]
1	-10	-8.37E-06
2	-6	-5.02E-06
3	-3	-2.51E-06
4	0	0
5	3	2.51E-06
6	6	5.02E-06
7	10	8.37E-06

Figure 5-8 demonstrates that the simulated temperature along the horizontal direction closely matched the analytical solutions in all the seven cases of the Peclet number. This agreement verified the steady heat transfer model of GeomechX.

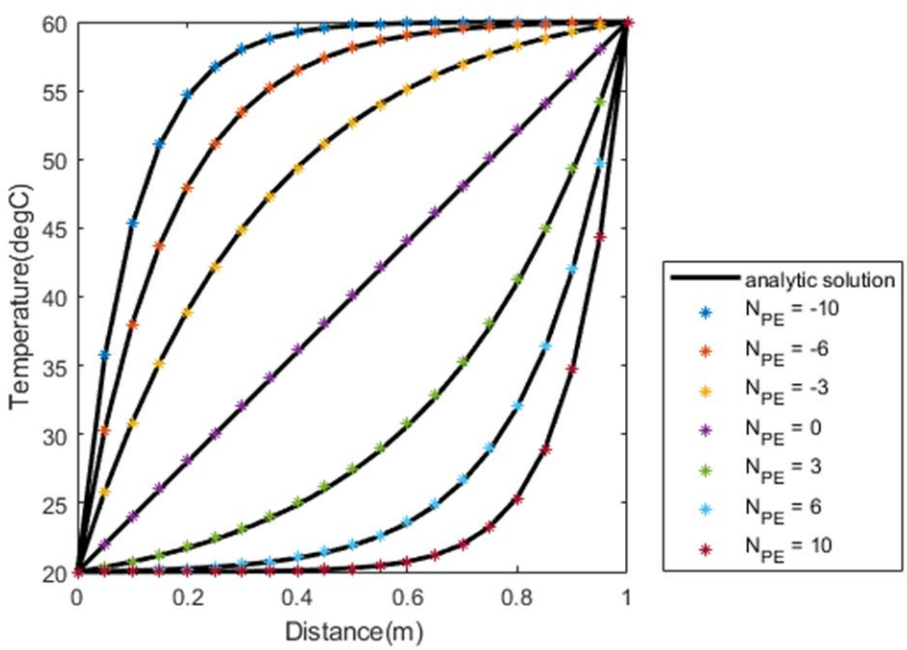

Figure 5-8 Temperature comparison to the analytical solutions in the seven

Peclet number cases. Colored points present the numerical solutions and black solid lines are the analytical solutions.

5.3.2 Transient heat diffusion equation

A verification of the transient heat transfer module was conducted focusing on heat conduction. For this verification, a semi-infinite solid was analyzed under two surface boundary conditions: constant surface temperature (Case 1) and constant surface heat flux (Case 2) (Figure 5-9). In Case 1, where the surface temperature is T_s, the analytical solution for temperature $T(x,\ t)$ at a location x at time t is expressed as:

$$\frac{T(x,\ t) - T_s}{T_i - T_s} = erf(\frac{x}{2\sqrt{\alpha t}}) \tag{5-9}$$

where T_i is the initial temperature, α is the thermal diffusivity. For Case 2, where the surface boundary has a constant heat flux ($q_s'' = q_0''$), the analytical solution is:

$$T(x,t) = T_i + \frac{2q_0''(\alpha t/\pi)^{1/2}}{k} exp\left(\frac{-x^2}{4\alpha t}\right) - \frac{q_0'' x}{k} erfc(\frac{x}{2\sqrt{\alpha t}}) \tag{5-10}$$

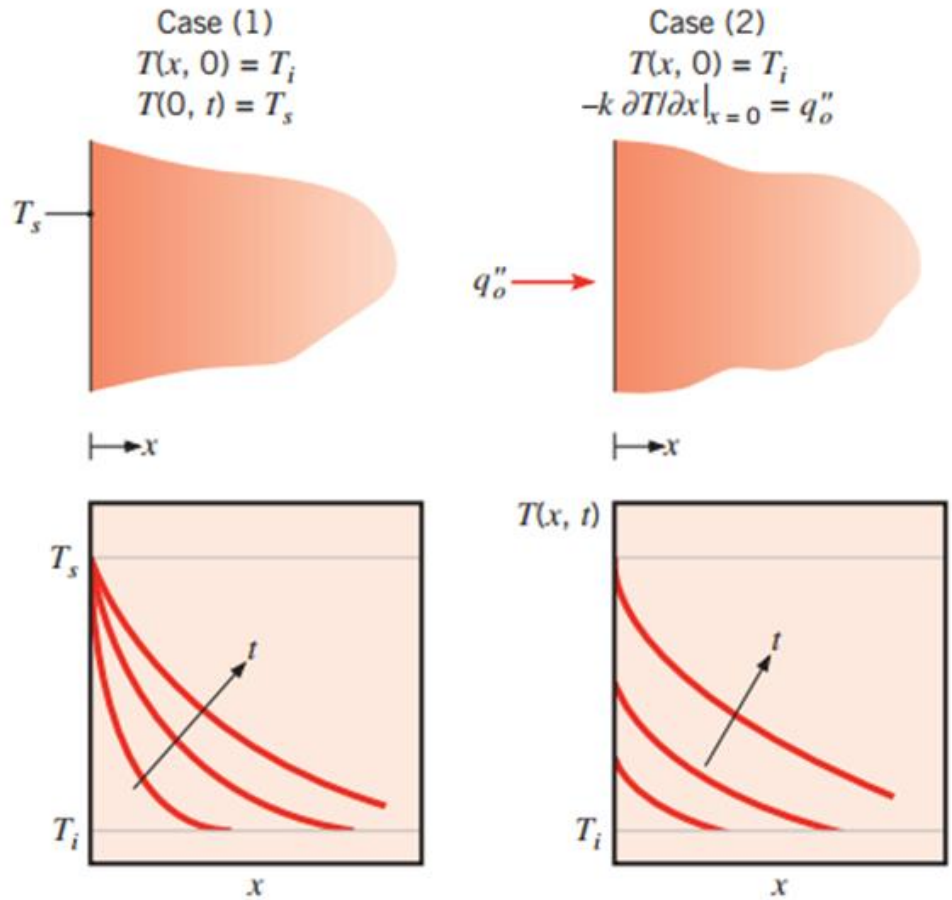

Figure 5-9 Transient temperature distributions in a semi-infinite solid under two surface conditions (Bergman, 2011).

To approximate the semi-infinite geometry, two- and three-dimensional models were constructed, elongated along the x-axis (Figure 5-10). For both models, boundary conditions of constant temperature (Case 1) or constant heat flux (Case 2) were applied at x=0 with the initial temperature set throughout the domain as specified in Table 5-4. All other boundaries were set as insulated. The simulations covered a period of one year. Additional model setup details are provided in Table 5-5.

(a)

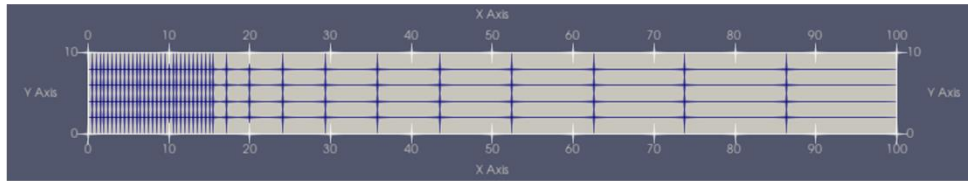

(b)

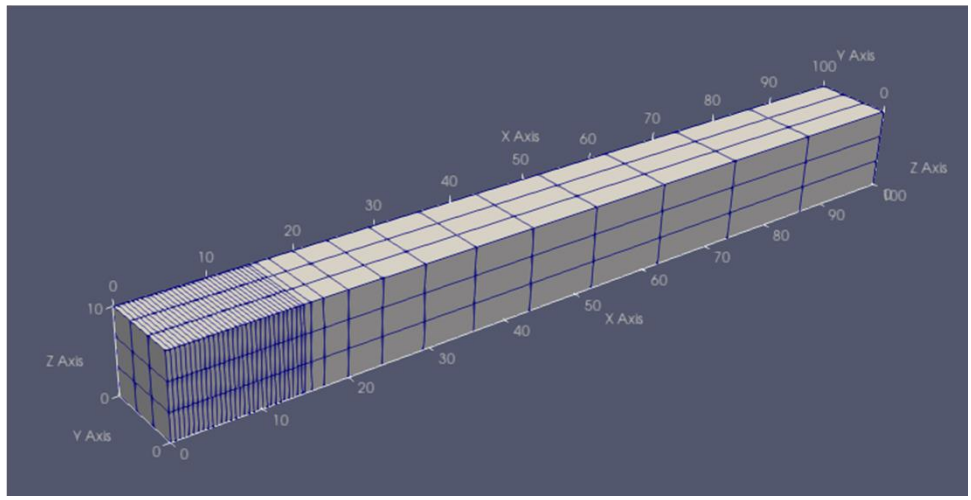

Figure 5-10 Model geometry and mesh details for (a) 2D and (b) 3D models.

Table 5-4 Boundary and initial conditions for Cases 1 and 2.

	Case 1	Case 2
Boundary condition at x=0	T = 15 ℃	$q_s'' = 10\ W/m^2$
Initial temperature	100 ℃	20 ℃

Table 5-5 Model setup for the transient heat transfer verification study.

		2D model	3D model
Geometry	Model size	100 m × 10 m	100 m × 10 m × 10 m
	Number of elements	210 (42 × 5)	378 (42 × 3 × 3)
Boundary condition	Insulation	x=100, y=0, and y=10	x=100, y=0, y=10, z=0, and z=10
Material property	Density ($\mathrm{kg/m^3}$)	2,700	
	Heat capacity (J/kg K)	800	
	Thermal conductivity (W/m K)	3.5	
Time		0 – 365 days	

Simulated temperatures along the x-axis were captured at various time intervals. In both Cases 1 and 2, the numerical results showed excellent agreement with the analytical solutions (Figure 5-11). This comparison verifies the capability of GeomechX in accurately simulating transient heat diffusion.

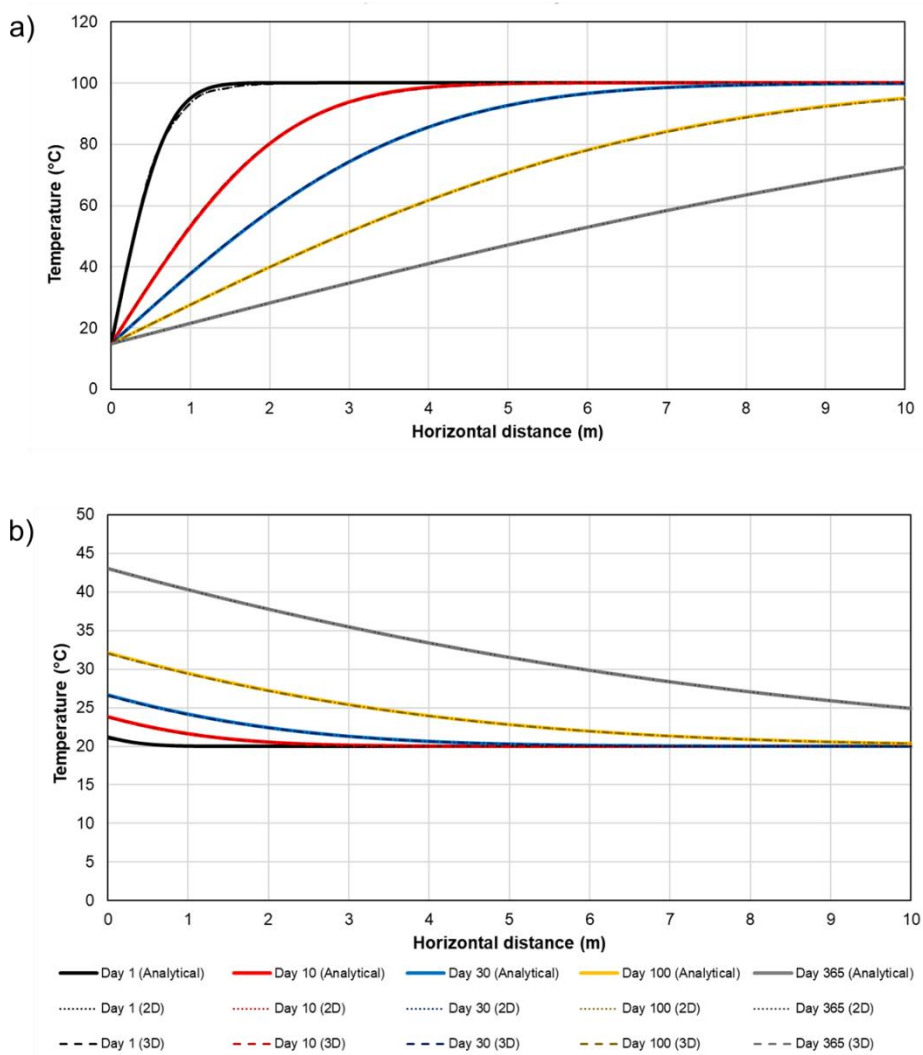

Figure 5-11 Comparison of numerical and analytical solutions for temperature along the horizontal direction at different times: a) constant surface temperature (Case 1) and b) constant surface heat flux (Case 2).

5.3.3 Transient heat conduction-convection

Verification of the transient heat conduction and convection module was performed by comparing results with a two-dimensional analytical solution for a rectilinear fracture model (Gringarten et al., 1975). This solution assumes that fluid is injected at a constant mass rate and temperature into multiple parallel fractures with uniform spacing (Figure 5-12). When fluid flows in the x-direction through fractures that are perpendicular to the z-direction, the transient temperatures of the rock and fluid can be calculated using the following equation:

$$T_D(x_D,\, z_D,\, s) = \frac{1}{s} exp\left[-x_D\sqrt{s} * tanh\left(\beta D_{ED}\sqrt{s}\right)\right] \cdot \left[cosh\left(\beta z_D\sqrt{s}\right) - tanh\left(\beta D_{ED}\sqrt{s}\right) sinh\left(\beta z_D\sqrt{s}\right)\right] \quad (5-11)$$

where T_D is the Laplace transform of dimensionless temperature, x_D and z_D are the dimensionless x and z coordinates, s is the Laplace parameter, D_{ED} is the dimensionless half-spacing, H is an arbitrary value for dimensionless forms, and β is defined as:

$$\beta = \frac{c_w Q}{2kHNW} \quad (5-12)$$

where c_w is the specific heat of fluid, Q is the total mass flow rate, k is the thermal conductivity of rock, N is the number of fractures, and W is the fracture width. The analytical solution was obtained using a simulator developed by Park et al. (2018), which incorporates Gringarten's solution.

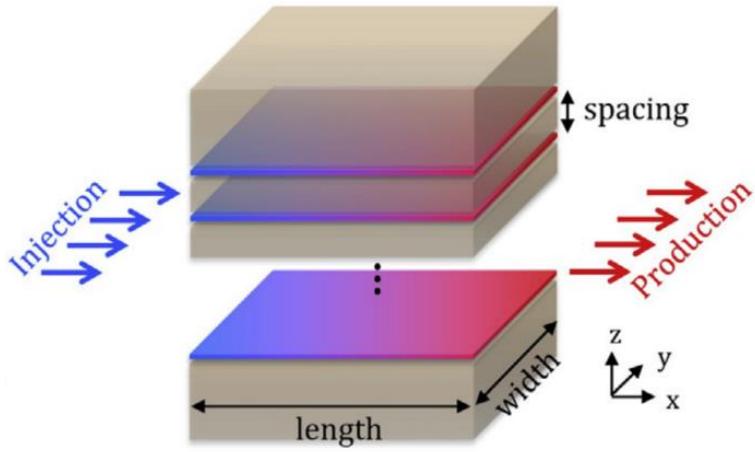

Figure 5-12 Schematic of the rectilinear fracture model used in Gringarten et al. (1975) (adapted from Park et al., 2018).

The injection and temperature conditions for this problem are summarized in Table 5-6. The setup assumes seven parallel fractures with uniform spacing of 70 m, with fracture planes having a length and width of 600 m. Equal injection rates were applied to all fractures.

Table 5-6 Properties used for the verification of transient heat conduction and convection.

Properties		Values
Temperature	Initial temperature (℃)	150
	Injection temperature (℃)	60
Rock property	Density, ρ_r $(\mathrm{kg/m^3})$	2,700
	Heat capacity, $c_{p,r}$ (J/kg K)	800
	Thermal conductivity, k_r (W/m K)	3.5
Fluid property	Density, ρ_f $(\mathrm{kg/m^3})$	1,000
	Heat capacity, $c_{p,f}$ (J/kg K)	4,200
	Number of fractures	7
	Fracture spacing (m)	70
	Length of fractures (m)	600
	Width of fractures (m)	600
	Time (years)	0 – 30

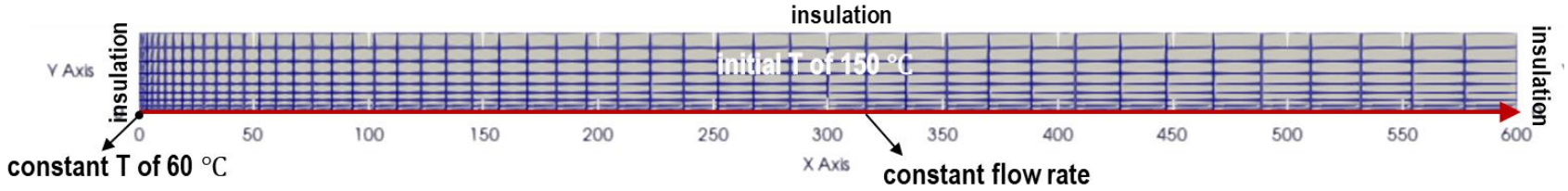

Figure 5-13 Geometry and initial and boundary conditions for the numerical model used in the verification of transient heat conduction and convection.

To simplify the numerical modeling, a single fracture with half-spacing was considered based on symmetry, as shown in Figure 5-13. Four cases of total mass flow rates—20, 40, 60, and 80 kg/s—were tested, corresponding to per-fracture flow rates of 2.857, 5.714, 8.571, and 11.429 kg/s, respectively. The details of the numerical model setup are provided in Table 5-7. The simulation results, including temperature along the fracture after 30 years and production temperature from 0 to 30 years, showed strong agreement with the analytical solution (Figure 5-14).

Table 5-7 Numerical model settings for the verification of transient heat conduction and convection.

Properties		**Values**
Geometry	Model size (m)	600 × 35
	Number of elements	561 (51 × 11)
Boundary condition	Insulation boundary	x=0, x=600, and y=35
	Constant fluid flow boundary	in the x direction at y=0
	Constant temperature	60 ℃ at point (0, 0)
Initial condition	Domain temperature (℃)	150

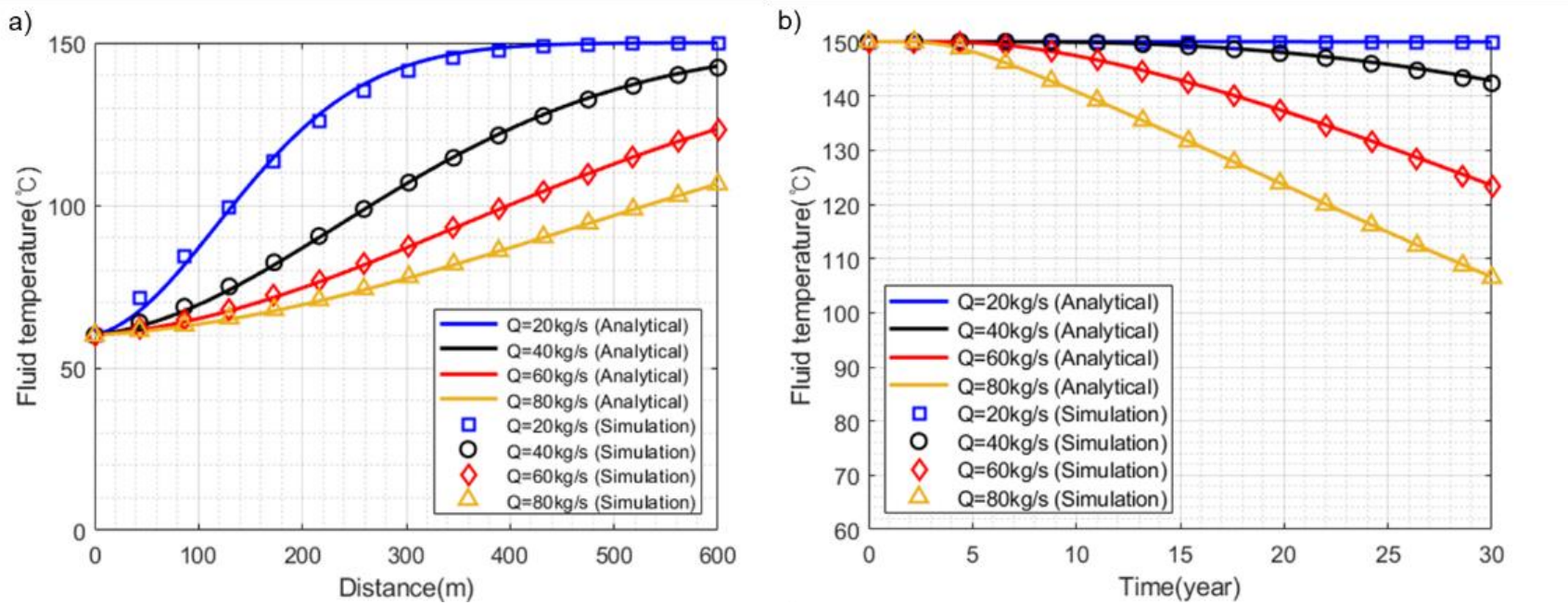

Figure 5-14 Verification of transient heat conduction and convection compared to the analytical solution by Gringarten et al. (1975): (a) Temperature along the fracture at 30 years and (b) Production temperature from 0 to 30 years.

5.4. Hydraulic process

A verification of the transient hydraulic module was performed to assess its capability in simulating pore pressure evolution. In this problem, a semi-infinite geometry was analyzed under two surface boundary conditions: constant pore pressure (Case 1) and constant injection at a Darcy's velocity (Case 2) (Figure 5-15). In Case 1, where the constant boundary pore pressure is P_0, the analytical solution for pore pressure $P_p(x, t)$ at a location x at time t is expressed as:

$$P_p(x,t) = P_i + P_0\, erfc\left(\frac{x}{\sqrt{4Dt}}\right) \tag{5-13}$$

where P_i is the initial domain pore pressure, and D is the hydraulic diffusivity given as $D = \frac{k}{\phi\mu C}$. For Case 2, where the surface boundary has injection at a constant Darcy's velocity of q_0, the analytical solution is:

$$P_p(x,t) = P_i + \frac{2q_0(Dt/\pi)^{1/2}}{k} exp\left(\frac{-x^2}{4Dt}\right) - \frac{q_0 x}{k} erfc\left(\frac{x}{2\sqrt{Dt}}\right) \tag{5-14}$$

To approximate the semi-infinite geometry, a two-dimensional model was built, elongated along the x-axis. Boundary conditions of constant pore pressure (Case 1) or constant injection rate (Case 2) were applied at x=0, with an initial pore pressure of zero throughout the domain. Additional model setup details are summarized in Table 5-8.

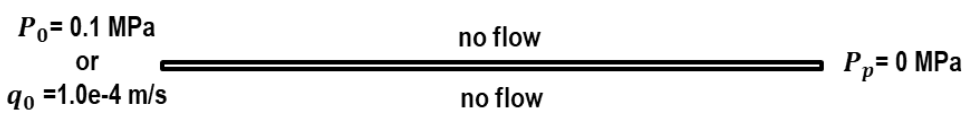

Figure 5-15 Schematic of the verification model of the hydraulic process.

Table 5-8 Model setup for the verification study of the hydraulic process

Properties	**Values**	
Model size	100m * 1m (2D)	
Number of elements	165	
Time	0 – 100,000 sec	
Initial pressure	0 Pa	
Boundary condition		
y=0, and y=1	No flow	
x=100	0 Pa	
x=0	Case 1 P_0= 0.1 Mpa	Case 2 q_0 =1.0e-4 m/s
Material property		
Compressibility (1/Pa)	5e-10	
Porosity	0.05	
Permeability (m^2)	1e-16	1e-14
Fluid density (kg/m^3)	1,000	
Fluid viscosity (Pa s)	0.001	

Simulated pore pressure along the x-axis were captured at various time intervals. For both Cases 1 and 2, the numerical results showed excellent agreement with the analytical solutions (Figure 5-16). This comparison verifies the ability of GeomechX to accurately simulate transient hydraulic behavior in porous media.

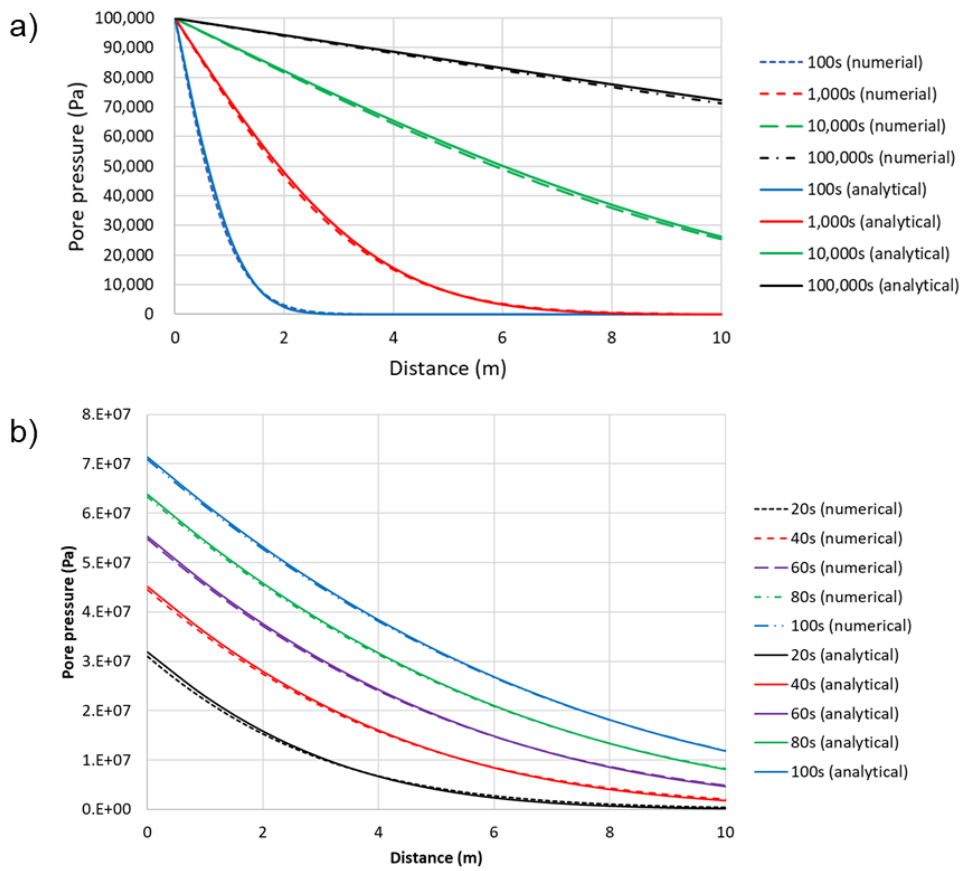

Figure 5-16 Comparison of numerical and analytical solutions for pore pressure along the horizontal direction at different times: a) constant surface pore pressure (Case 1) and b) constant injection rate (Case 2).

5.5. Thermo-mechanical coupled process

The thermo-mechanical coupled process of the code was verified by conducting an example modeling and comparing the results with those from a commercial FEM software, COMSOL Multiphysics. The study simulated transient heat conduction and thermally induced stress and displacement in a two-dimensional model under a plane strain condition. The model was 0.1 m $\times$ 1 m, composed of 116 triangular elements. The material properties of the model are given in Table 5-9. The initial and boundary conditions were described in Figure 5-17. A uniform initial temperature was given to the domain. the left and right boundaries were insulated and the bottom boundary had a constant temperature equal to the initial domain temperature. The left, right, and bottom boundaries were under roller boundary conditions while the top boundary was free to move. On the top boundary a constant temperature greater by 1 degree than the initial domain temperature was applied. The temperature evolution and consequent mechanical behaviors were monitored over 200 hours.

The finite element approximation order was set to two for both displacement and temperature. The generalized minimal residual method (GMRES) was employed with LU factorization preconditioning. Time stepping was performed using the backward differentiation formula (BDF) of order two, with the default time step adaptor provided by the TS class in PETSc.

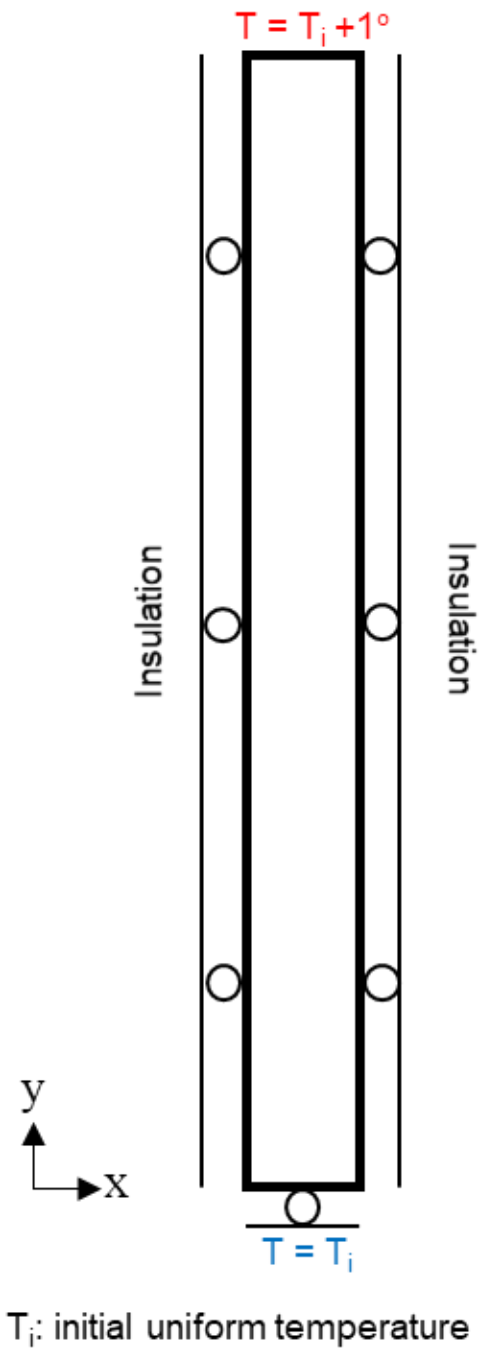

Figure 5-17 Schematic of the transient thermo-mechanical coupled model.

Table 5-9 Material properties applied to the thermo-mechanical coupled model for verification.

Properties	Values
Young's modulus (GPa)	30
Poisson's ratio	0.2
Linear thermal expansion coefficient (1/℃)	5e-6
Density, ρ_r $(\mathrm{kg/m^3})$	2500
Heat capacity, $c_{p,r}$ (J/kg K)	800
Thermal conductivity, k_r (W/m K)	3.0

The comparison of the results between this code and COMSOL Multiphysics was conducted as shown in Figure 5-18. The temperature distribution along the y direction of the model showed agreement with the commercial software at different points of time (Figure 5-18a). Consequently, the thermal stress was generated as the model was confined in the x direction, and normal strain in the y direction was observed. The modeled results of the normal stress in the x direction and normal strain in the y direction matched well with those from the commercial software (Figure 5-18b and c). The vertical displacement was monitored at the top of the model over the simulation time as described in Figure 5-18d. The upward displacement due to thermal expansion also agreed well with the values from the commercial simulator.

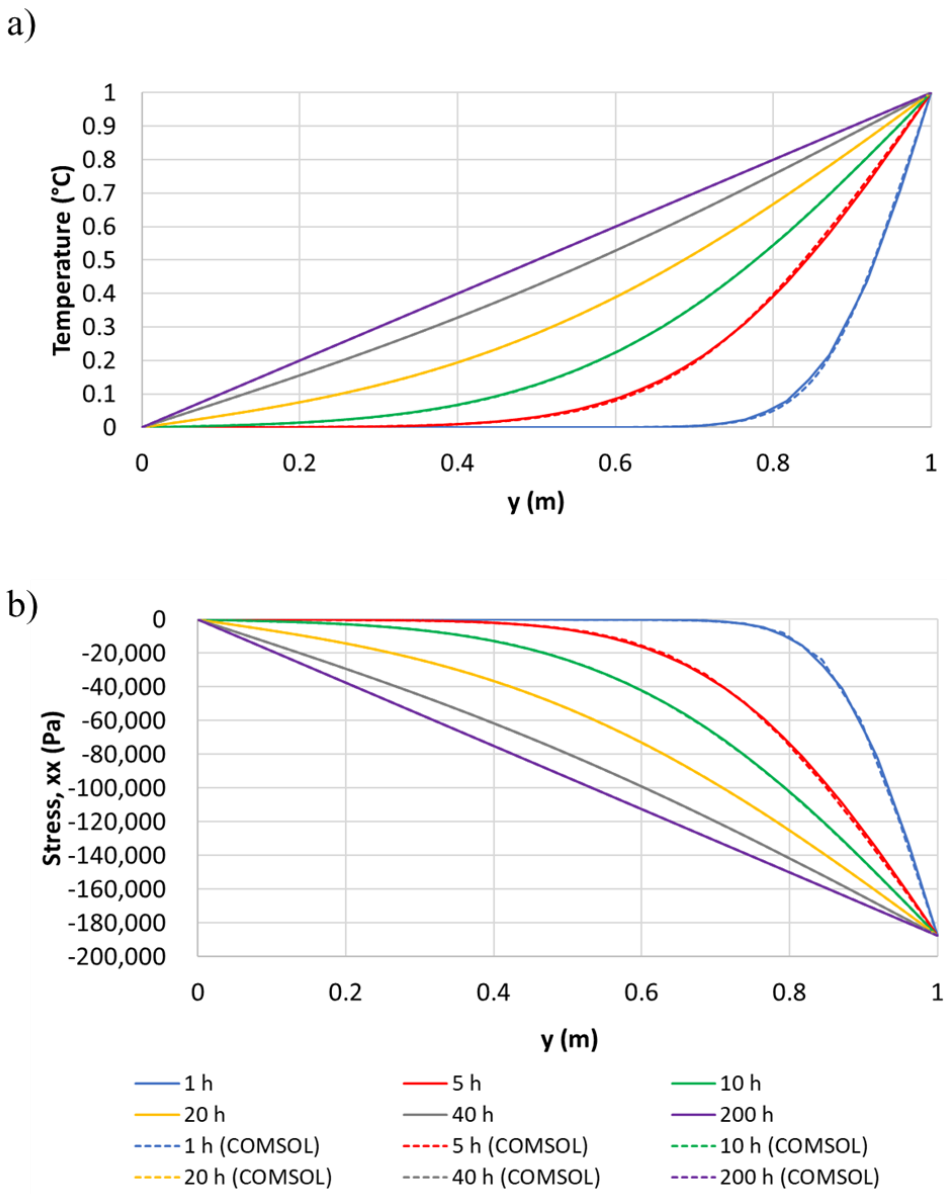

Figure 5-18 Comparison of the results of the coupled thermo-mechanical model with COMSOL Multiphysics. a) Temperature, b) normal stress in the x direction, and c) normal strain in the y direction monitored along the vertical axis of the model. d) the y displacement measured at the top boundary from 0 to 200 hours.

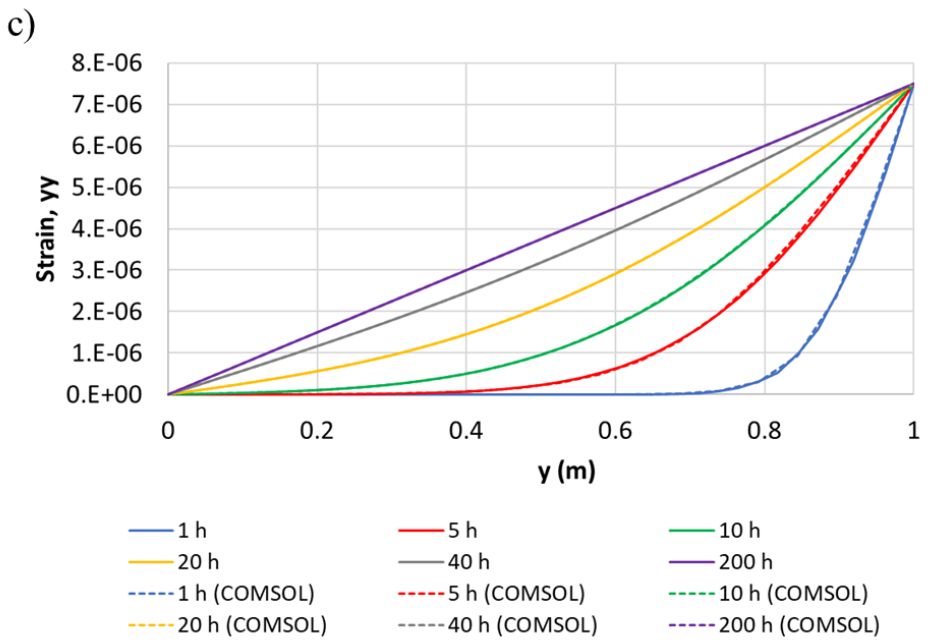

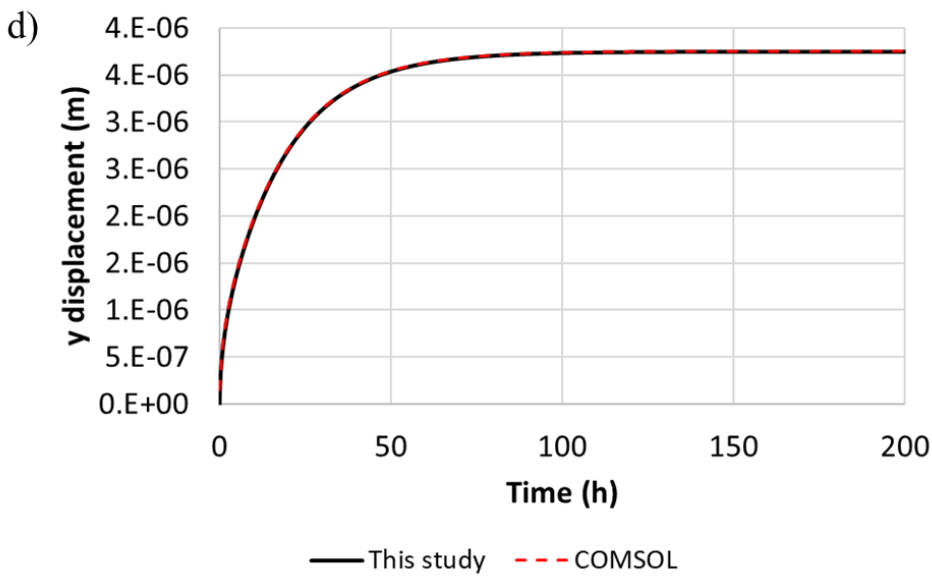

Figure 5-18 Comparison of the results of the coupled thermo-mechanical model with COMSOL Multiphysics. a) Temperature, b) normal stress in the x direction, and c) normal strain in the y direction monitored along the vertical axis of the model. d) the y displacement measured at the top boundary from 0 to 200 hours.

5.6. Hydro-mechanical coupled process

This chapter presents two verification cases for transient HM coupled processes with comparison to analytical solutions.

5.6.1 Terzaghi (1923)

The one-dimensional consolidation problem (Terzaghi, 1923) was performed to verify the accuracy of the hydro-mechanical coupling code. For the verification, two- and three- dimensional cases were modeled. A compressive normal load of 10 Pa was applied at the upper surface of the undrained poroelastic model. The other surfaces were confined to roller and no flow boundary conditions. The vertical length was assumed to be 10 m (Figure 5-19). The material properties were applied as shown in Table 5-10.

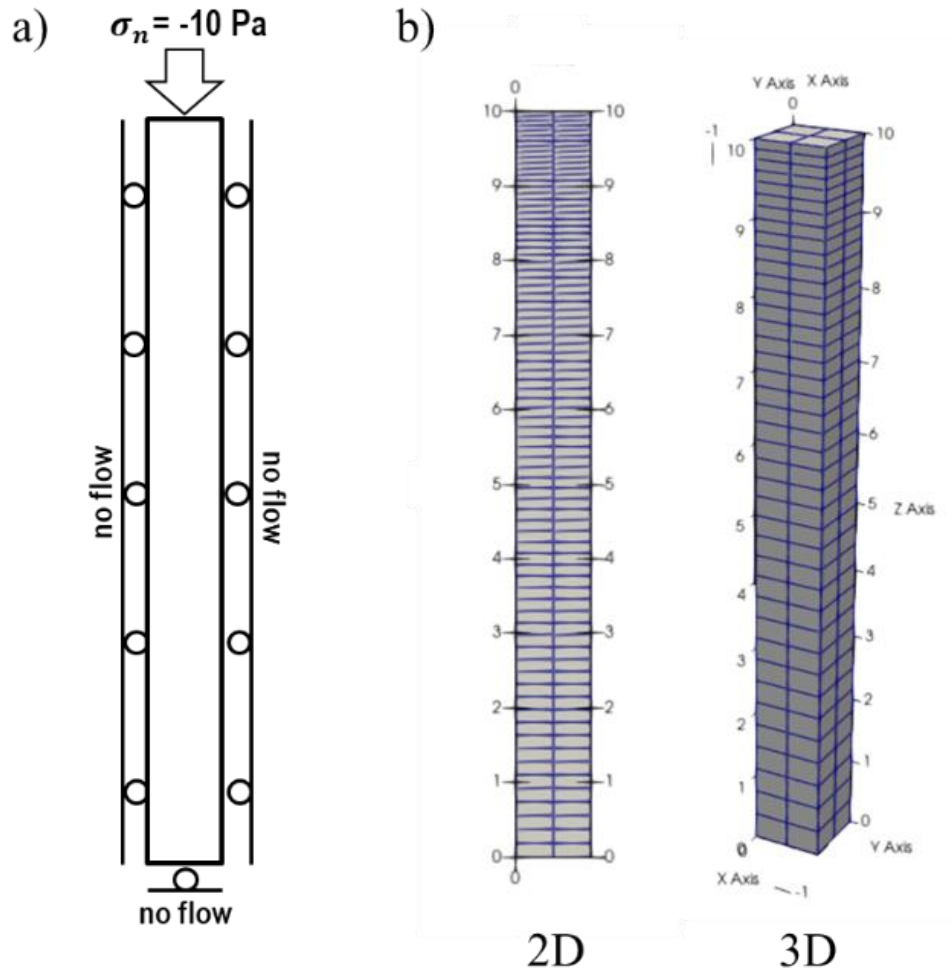

Figure 5-19 The hydro-mechanical coupled model for verification. a) Boundary conditions. b) Mesh of the two- and three-dimensional models.

Table 5-10 Material properties applied to the one-dimensional consolidation model for verification.

Properties	Values
Bulk modulus (GPa)	13.0
Shear modulus (GPa)	13.0
Permeability (m^2)	2e-16
Fluid density (kg/m^3)	1,000
Fluid viscosity (Pa s)	0.001
Biot modulus (GPa)	41.0
Biot coefficient	0.65

The analytical solution for the excess pore pressure at depths of z is given by the below equation:

$$P_p(z,t) = -\frac{\alpha M \sigma_n}{\lambda + 2G + \alpha^2 M} \sum_{n=1,3,\dots}^{\infty} \frac{4}{n\pi} sin\left(\frac{n\pi z}{2h}\right) exp(-\frac{n^2\pi^2 kt}{4\mu Sh^2}) \quad (5-15)$$

where h is the vertical length of the model, σ_n is the normal stress with tension (+) notation, and t is the time. An excess pore pressure was instantaneously induced due to the Skempton effect, and it gradually drained out over time. The vertical displacement at the upper surface can be calculated by

$$w(t) = \frac{\sigma_n h}{\lambda + 2G} \left[1 - \frac{\alpha^2 M}{\lambda + 2G + \alpha^2 M} \sum_{n=1,3,\dots}^{\infty} \frac{8}{n^2\pi^2} exp\left(\frac{-n^2\pi^2 kt}{4\mu Sh^2}\right)\right] \quad (5-16)$$

The finite element method used an approximation order of one for displacement, pressure, and volumetric strain, with quadrilateral elements in 2D and hexahedral elements in 3D. The generalized minimal residual method (GMRES) was applied, utilizing LU factorization for preconditioning. Time integration was conducted with the implicit backward Euler method, using the default time step adaptor available in the TS class of PETSc.

The simulated excess pore pressure was compared with the analytical

solution along the vertical direction at different times as presented in Figure 5-20a. The vertical displacement at the upper surface initially had the value corresponding to the undrained condition and the amount increased as it reached the drained state (Figure 5-20b). Both of the simulated excess pore pressure and vertical displacement matched the analytical solutions.

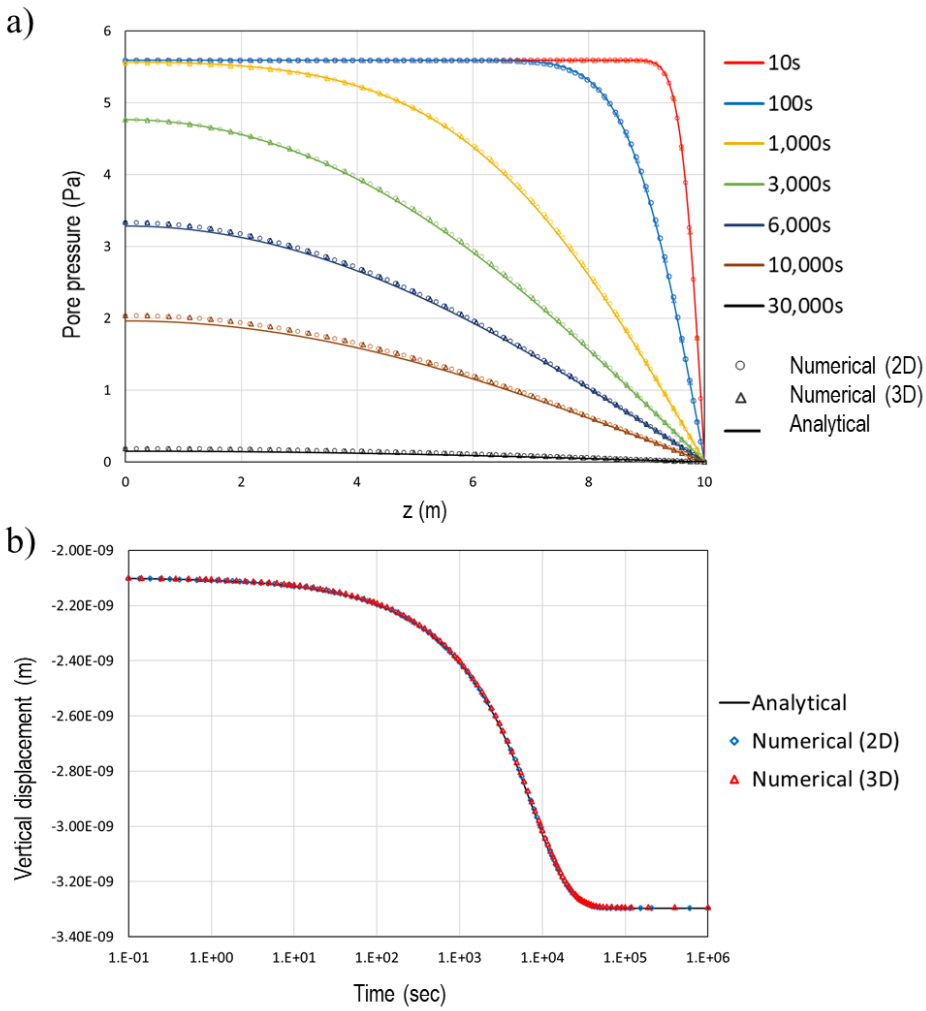

Figure 5-20 Comparison between the analytical solutions and simulated results from the two- and three-dimensional models. a) Excess pore pressure along the vertical direction at different times. b) Vertical displacement at the top boundary.

5.6.2 Cryer (1963)

Cryer (1963) studied the behavior of a saturated porous sphere subjected to a suddenly applied constant radial compressive stress. In the Cryer problem, the sphere's surface is permeable, allowing fluid to escape freely. This problem demonstrates the non-monotonic pore pressure diffusion phenomenon, known as the Mandel-Cryer effect. Upon loading, the Skempton effect generates a uniform increase in pore pressure. As the pressure begins to dissipate near the sphere's surface, the outer layer softens. Due to compatibility requirements, the load is transferred to the inner, relatively stiffer material, causing an additional rise in pore pressure within the sphere's interior (Detournay & Cheng, 1993). Consequently, during the early stages of consolidation, the pore pressure at the center of the sphere initially increases further after the instantaneous rise caused by the Skempton effect, before eventually dissipating due to pressure diffusion.

The initial condition assumes an undisturbed specimen, and at t = 0^+, a radial stress P_0 is suddenly applied to the sphere surface. The boundary conditions are as follows:

$$\begin{aligned} &\sigma_{RR} = -P_0 H(t) \text{ and } p_p = 0 \text{ at } R = R_0 \\ &u_R = 0 \text{ and } \frac{\partial p_p}{\partial R} = 0 \text{ at } R = 0 \end{aligned} \tag{5-17}$$

where the subscript R refers to the radial direction and R_0 represents the radius of the sphere.

For a porous medium composed of incompressible solid and fluid constituents, the pore pressure at a radius R and time t, denoted as $p_p(R,t)$, is expressed as:

$$\frac{p_p(R,t)}{P_0} = \sum_{n=1}^{\infty} \frac{4(1-\nu)(1-2\nu)[\sin(R^*\sqrt{x_n}) - R^*\sin\sqrt{x_n}]}{[(1-\nu)^2 x_n - 2(1+\nu)(1-2\nu)]R^*\sin\sqrt{x_n}} e^{-x_n t^*} \tag{5-18}$$

Here, the dimensionless parameters are defined as $R^* = R/R_0$ and $t^* = ct^2/R_0^2$, where c is the coefficient of consolidation:

$$c = \frac{3K(1-\nu)}{(1+\nu)}\frac{k}{\mu} \tag{5-19}$$

The roots x_n are the positive solutions of the algebraic equation:

$$\tan\sqrt{x_n} = \frac{2(1-2\nu)\sqrt{x_n}}{2(1-2\nu)-(1-\nu)x_n} \tag{5-20}$$

For the verification study, one-eighth of a sphere with a radius of 1 m was modeled, considering the symmetry of the sphere (Figure 5-21). A compressive normal stress of 1 Pa and a pore pressure of 0 Pa were applied to the sphere's surface. Roller and no-flow boundary conditions were applied to the three symmetry planes. The material properties listed in Table 5-11 were used, and a relatively high Biot modulus was assumed to approximate incompressibility.

Table 5-11 Material properties applied to the Cryer model for verification.

Properties	Values
Bulk modulus (GPa)	20.0
Shear modulus (GPa)	12.0
Poisson's ratio	0.25
Permeability (m^2)	2e-16
Fluid density (kg/m^3)	1,000
Fluid viscosity (Pa·s)	0.001
Biot modulus (GPa)	4.1e5
Biot coefficient	1.0

The finite element approximation order was set to two for displacement and one for pressure and volumetric strain, using tetrahedral elements. The generalized conjugate residual method (GCR) was employed with LU factorization preconditioning, incorporating a diagonal shift to avoid zero pivots. Time stepping was performed using the implicit backward Euler method with the default time step adaptor provided by the TS class in PETSc.

The Mandel-Cryer effect was successfully captured in the numerical model, demonstrating an initial pressure increase at the center followed by a subsequent decline. The simulated pressure evolution at the center showed excellent agreement with the analytical solution, as illustrated in Figure 5-22.

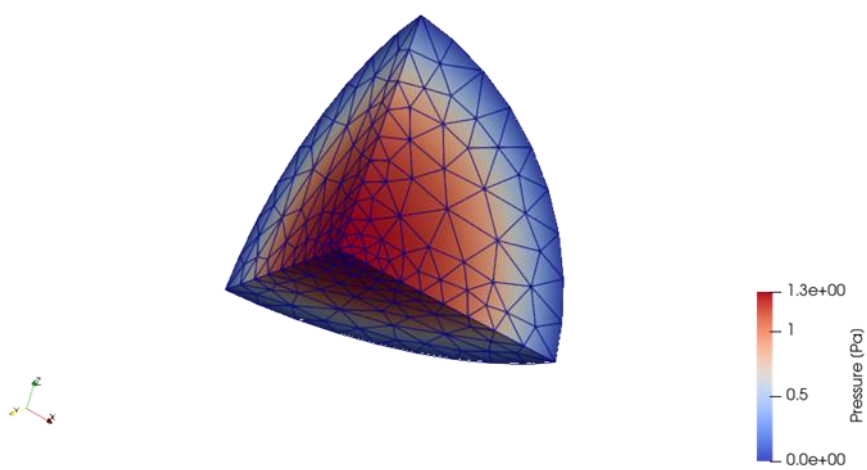

Figure 5-21 Pore pressure distribution at t = 6.1 seconds (t* = 0.044).

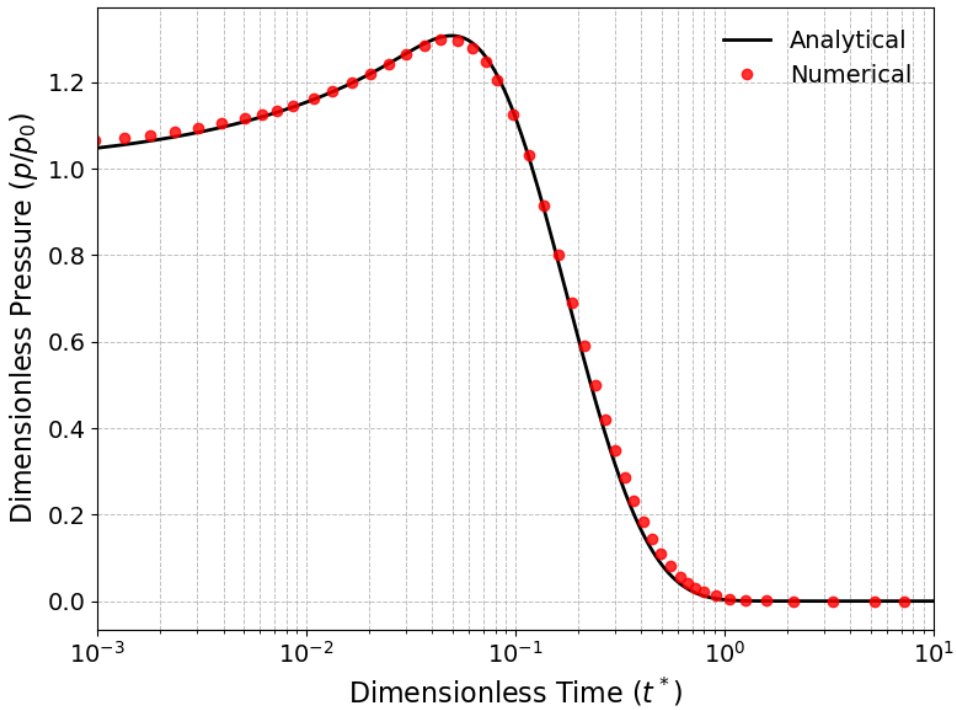

Figure 5-22 Comparison of analytical and numerical solutions for dimensionless pore pressure at the center of the sphere over time.

5.7. Thermo-hydro-mechanical coupled process

This chapter presents two verification cases for transient THM coupled processes with comparison to analytical solutions.

5.7.1 McTigue (1986)

McTigue (1986) developed a linear thermoporoelastic theory for saturated media, incorporating fluid compressibility and thermal expansion, and providing analytical solutions for one-dimensional heating of a half-space. In terms of the heat transfer through the domain, the solution considered only heat conduction without convection.

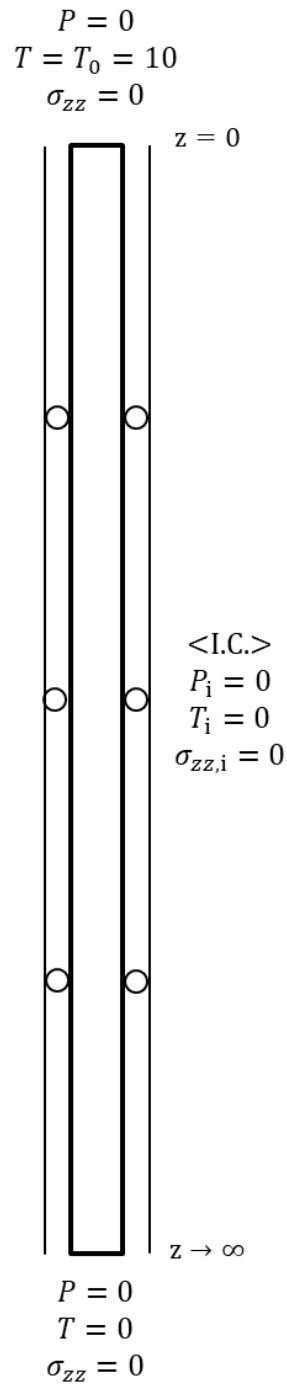

Figure 5-23 Initial and boundary conditions of the verification model of linear thermoporoelasticity (McTigue, 1986).

This benchmark case was numerically modeled and compared with the numerical results with the analytical solutions. The material properties of Abyssal red clay and rock salt (Cheng, 2016), typical rock types in geomechanics, were tested for the verification (Table 5-12). Figure 5-23 illustrates the initial and boundary conditions applied to a two-dimensional model with a size of 1 m by 100 m. Heating was applied along the top boundary, with a constant temperature 10°C higher than the initial domain temperature. Drained and free displacement boundary conditions were applied on the top boundary, while roller boundaries were applied on the vertical boundaries.

The finite element approximation order was set to two for displacement, temperature, and pressure and one for volumetric strain, using quadrilateral elements. The generalized minimal residual method (GMRES) was employed with a diagonally scaled system. For preconditioning, a fieldsplit block preconditioner with multiplicative composition was applied. Specifically, block Jacobi preconditioning was used for the pressure, temperature, and volumetric strain fields, while LU factorization was applied for displacement. Time stepping was performed using the implicit backward Euler method, utilizing the default time step adaptor provided by the TS class in PETSc.

Table 5-12 Material properties used in the benchmark study of McTigue (1986) for the THM verification (Cheng, 2016).

	Abyssal red clay	Rock salt
Drained bulk modulus (Pa)	2×10^7	2.07×10^{10}
Shear modulus (Pa)	7.2×10^4	1.2410^{10}
Biot modulus (Pa)	2.77×10^9	1.81×10^{11}
Porosity	0.71	0.001
Permeability (m^2)	3×10^{-16}	1×10^{-21}*
Fluid viscosity (Pa·s)	0.0015	0.001
Biot coefficient	1.0	0.119
Poisson's ratio	0.4982	0.25
Volumetric thermal expansion coefficient for fluid (1/K)	3.0×10^{-4}	3.0×10^{-4}
Volumetric thermal expansion coefficient for solid (1/K)	3.4×10^{-5}	1.2×10^{-4}
Equivalent volumetric heat capacity (J/m^3·K)	3.92×10^6	1.89×10^6
Equivalent thermal conductivity (W/m·K)	1.02	6.6

* Different values of permeability in Table 5-13 were applied according to diffusivity ratios for the verification of temperature and pressure solutions.

Table 5-13 Permeability values used according to different diffusivity ratios, $R = \sqrt{c/\kappa_T}$.

Diffusivity ratio	2.0	1.0	0.5	0.25	0.1
Permeability (m^2)	8.2485×10^{-20}	2.0621×10^{-20}	5.1553×10^{-21}	1.2888×10^{-21}	2.0621×10^{-22}

The numerical results had strong agreement with the analytical solutions. Figure 5-24a and b show that temperature changes due to heat conduction and pore pressure changes induced by the thermoporoelastic effects were successfully simulated at different diffusivity ratios, $R = \sqrt{c/\kappa_T}$, where c and κ_T are the coefficient of consolidation and thermal diffusivity, respectively. The higher the diffusivity ratio is, the pressure diffusion faster than heat conduction, and the pressure response smaller. Figure 5-24c and d illustrate the mechanical responses such as effective stress and displacement in the red clay and rock salt over time. The displacement due to thermal expansion of drained material and thermally induced pore pressure, which causes tensile stress and additional expansion, were effectively simulated. The latter effect was notable in red clay, while thermal expansion was evident in rock salt.

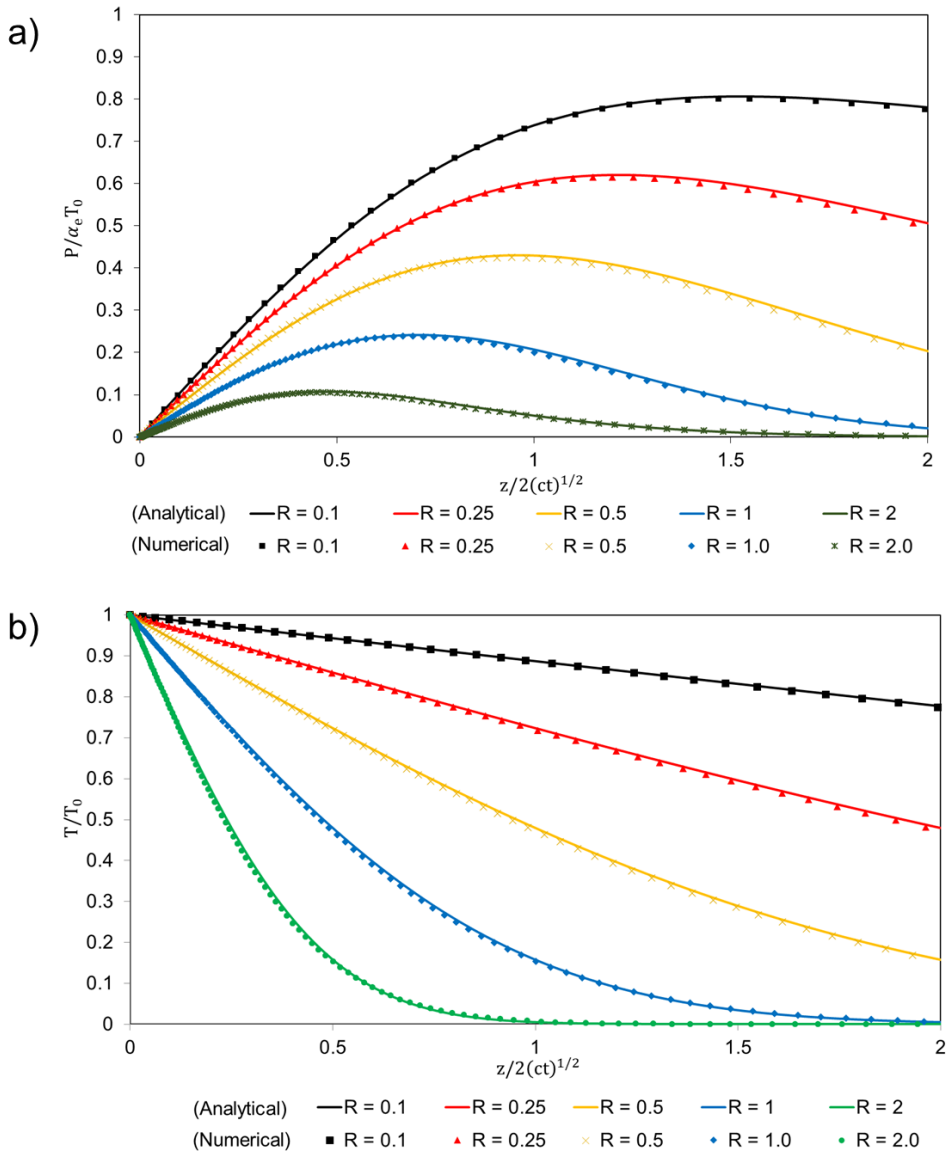

Figure 5-24 Verification of linear thermoporoelasticity by comparing numerical and analytical solutions from McTigue (1986): a) Pore pressure and b) temperature solutions for different diffusivity ratios, c) Horizontal effective stress versus vertical distance at different times, d) Vertical displacements over depth at 30 days.

.

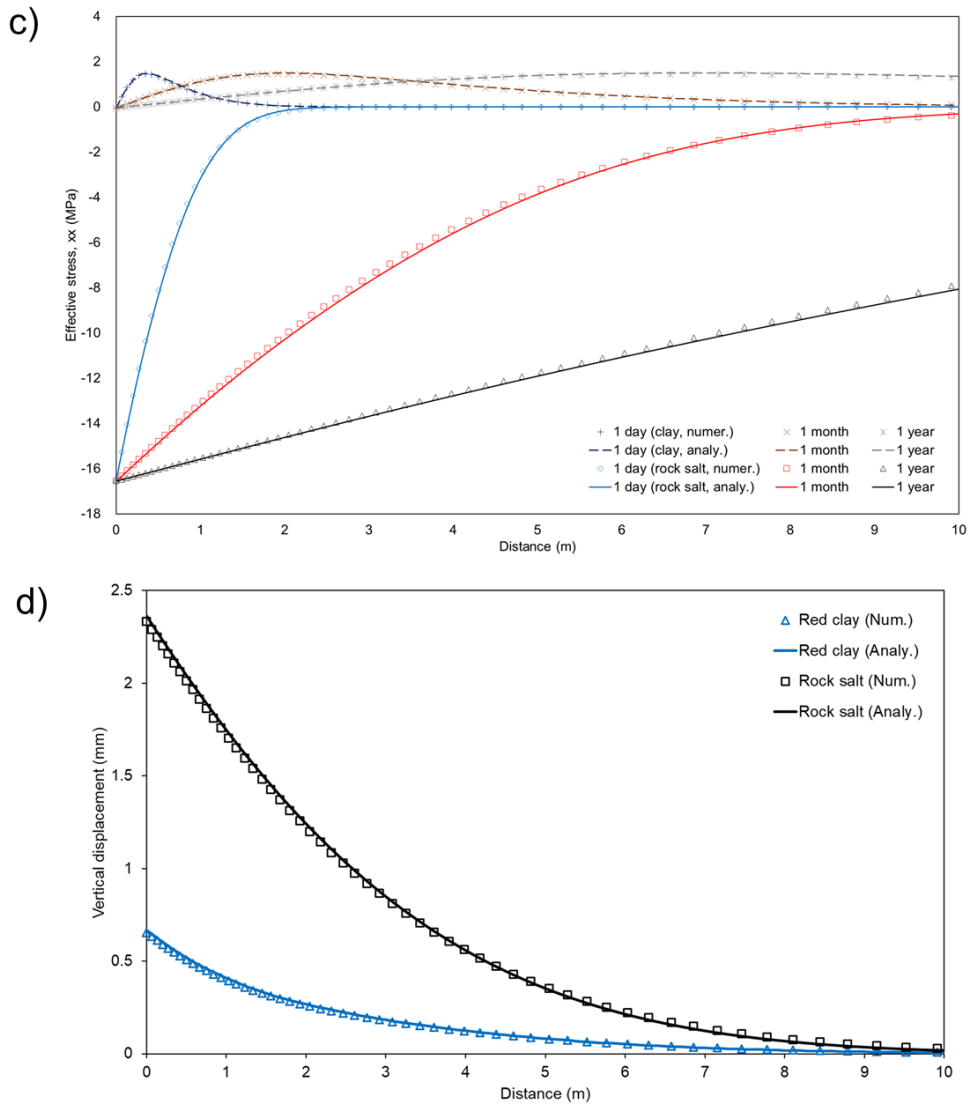

Figure 5-24 Verification of linear thermoporoelasticity by comparing numerical and analytical solutions from McTigue (1986): a) Pore pressure and b) temperature solutions for different diffusivity ratios, c) Horizontal effective stress versus vertical distance at different times, d) Vertical displacements over depth at 30 days.

5.7.2 Booker and Savvidou (1985)

Booker & Savvidou (1985) provided an analytical solution for thermoporoelastic consolidation in an infinite, homogeneous, isotropic, saturated porous medium surrounding a point heat source, considering only conductive heat transfer. The fluid and solid grains are assumed to be incompressible, so any variation in fluid mass occurs solely from mechanical deformations and the thermal expansion of the fluid and porous medium.

This benchmark case was numerically modeled applying a point heat source with a constant heat power of 800 W over one year. The material properties are presented in Table 5-14. To approximate incompressibility, a relatively large Biot modulus value of $5.0 \times 10^{13}\ Pa$ was used to minimize the influence of the first term in Eq. (4-19). As presented in Figure 5-25a, a 1/8 symmetry model was constructed with dimensions of 20 m × 20 m × 20 m with a heat source sized 0.01 m × 0.01 m × 0.01 m located at (0 m, 0 m, 0 m). Results were monitored at three points: P1 (0.9159 m, 1.201 m, 0.8308 m), P2 (0.4318 m, 0.4491 m, 0.3948 m), and P3 (0.2889 m, 0.1605 m, 0.08987 m).

The finite element method utilized tetrahedron elements, with an approximation order of two for displacement, temperature, and pressure, and one for volumetric strain. The generalized minimal residual method (GMRES) was used for solving the system, employing diagonal scaling. Preconditioning was implemented using a fieldsplit block preconditioner with multiplicative composition. In particular, block Jacobi preconditioning was applied to the pressure, temperature, and volumetric strain fields, while LU factorization was used for displacement. Time integration was carried out with the implicit backward Euler method, leveraging the default time step adaptor provided by the TS class in PETSc.

Table 5-14 Material properties used in the benchmark study of Booker and Savvidou (1985) for the THM verification.

	Values
Drained bulk modulus (Pa)	4×10^9
Shear modulus (Pa)	2.4×10^9
Biot modulus (Pa)*	5.0×10^{13}
Porosity	0.15
Permeability (m^2)	5×10^{-20}
Fluid viscosity (Pa·s)	0.001
Biot coefficient	1.0
Poisson's ratio	0.25
Volumetric thermal expansion coefficient for fluid (1/K)	3.0×10^{-4}
Volumetric thermal expansion coefficient for solid (1/K)	3.9×10^{-5}
Equivalent volumetric heat capacity ($J/m^3 \cdot K$)	2.47405×10^6
Equivalent thermal conductivity (W/m·K)	3.0

In Figure 5-25b and c, GeomechX accurately captures temperature increases and the rise and subsequent dissipation of pore pressure from thermal pressurization, showing excellent agreement with analytical results. The model simulates material expansion, as well as normal and shear stresses, resulting from combined increases in temperature and pressure. Notably, the model reflects the sustained displacements, demonstrating that residual expansion persists as long as elevated temperatures are maintained. Minor discrepancies in pore pressure and stress may result from subtle modeling factors, including the influence of the first term in Eq. (4-19) and boundary effects within the finite domain, in contrast to the infinite domain assumption in the analytical solution. Overall, these results confirm GeomechX's reliability in modeling thermoporoelastic responses with consistent alignment to analytical solutions.

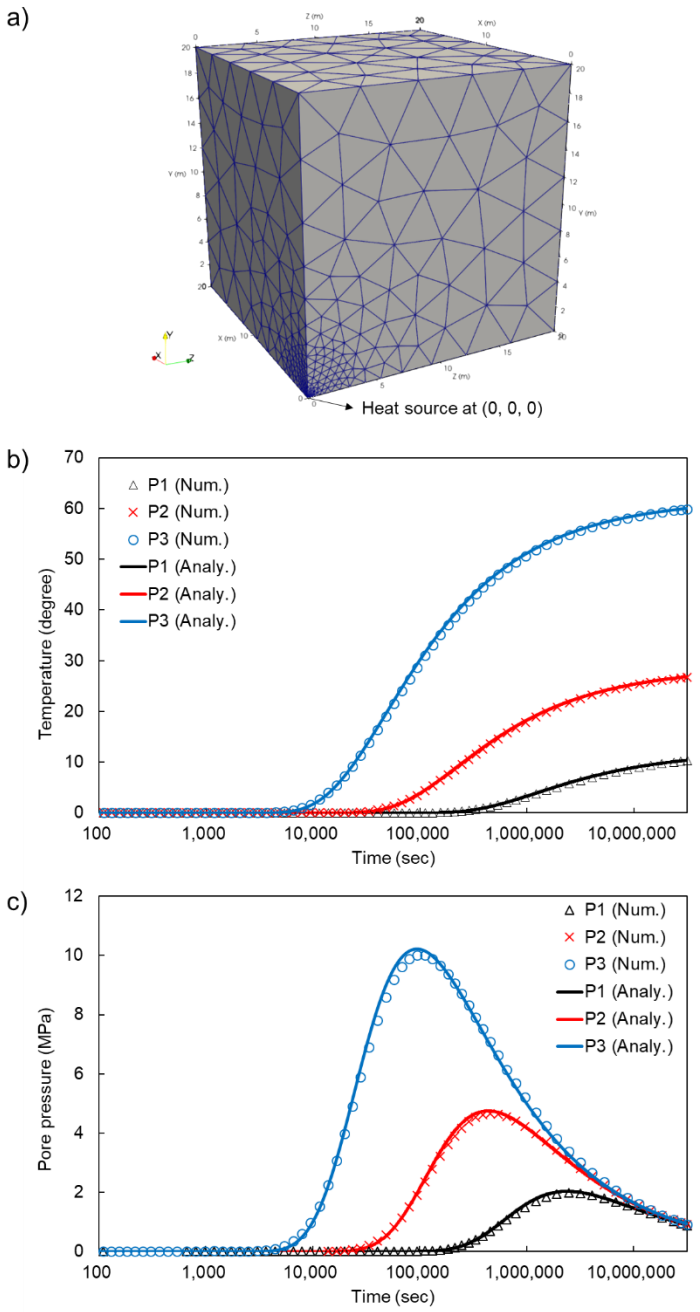

Figure 5-25 Verification of linear thermoporoelasticity in comparison to the solutions in (Booker & Savvidou, 1985). a) Model geometry. b-f) Comparison between the numerical and analytical solutions at three points (P1, P2, and P3) over one year: b) temperature, c) pore pressure, d) displacement, e) normal stress, and f) shear stress.

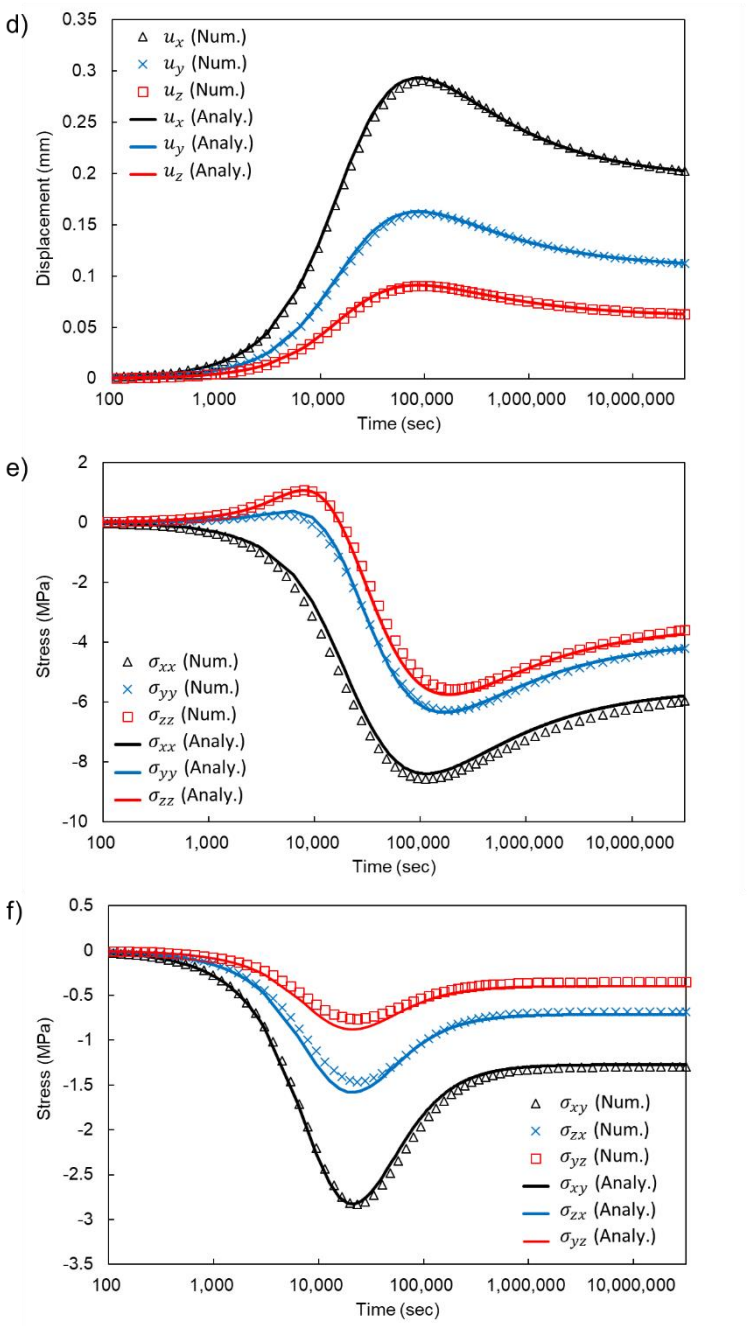

Figure 5-25 Verification of linear thermoporoelasticity in comparison to the solutions in (Booker & Savvidou, 1985). a) Model geometry. b-f) Comparison between the numerical and analytical solutions at three points (P1, P2, and P3) over one year: b) temperature, c) pore pressure, d) displacement, e) normal stress, and f) shear stress.

6. References

Bergman, T. L. (2011). *Fundamentals of heat and mass transfer*. John Wiley & Sons.

Booker, J. R., & Savvidou, C. (1985). Consolidation around a point heat source. *International Journal for Numerical and Analytical Methods in Geomechanics*, *9*(2), 173–184.

Cheng, A. H.-D. (2016). *Poroelasticity* (Vol. 27). Springer.

Cho, J. W., Kim, H., Jeon, S., & Min, K. B. (2012). Deformation and strength anisotropy of Asan gneiss, Boryeong shale, and Yeoncheon schist. *International Journal of Rock Mechanics and Mining Sciences*, *50*, 158–169. https://doi.org/10.1016/J.IJRMMS.2011.12.004

COMSOL. (2007). COMSOL multiphysics reference manual. *COMSOL AB*.

Cryer, C. W. (1963). A Comparison of the three-dimensional consolidation theories of Biot and Terzaghi. *The Quarterly Journal of Mechanics and Applied Mathematics*, *16*(4), 401–412. https://doi.org/10.1093/qjmam/16.4.401

Detournay, E., & Cheng, A. H.-D. (1993). Fundamentals of poroelasticity. In *Analysis and design methods* (pp. 113–171). Elsevier.

Gringarten, A. C., Witherspoon, P. A., & Ohnishi, Y. (1975). Theory of heat extraction from fractured hot dry rock. *Journal of Geophysical Research*, *80*(8), 1120–1124. https://doi.org/10.1029/jb080i008p01120

Jaeger, J. C., Cook, N. G. W., & Zimmerman, R. (2007). *Fundamentals of Rock Mechanics*. Wiley. https://books.google.co.kr/books?id=FqADDkunVNAC

Kirsch, E. G. (1898). Die Theorie der Elastizit t und die Bed rfnisse der Festigkeitslehre. *Zeitshrift Des Vereines Deutscher Ingenieure*, *42*, 797–807.

Knepley, M. G., Brown, J., Rupp, K., & Smith, B. F. (2013). *Achieving High Performance with Unified Residual Evaluation*. http://arxiv.org/abs/1309.1204

McTigue, D. F. (1986). Thermoelastic response of fluid-saturated porous rock. *Journal of Geophysical Research: Solid Earth*, *91*(B9), 9533–9542. https://doi.org/10.1029/jb091ib09p09533

Park, S., Kim, K.-I., Kwon, S., Yoo, H., Xie, L., Min, K.-B., & Kim, K. Y. (2018). Development of a hydraulic stimulation simulator toolbox for enhanced geothermal system design. *Renewable Energy*, *118*, 879–895.

Terzaghi, von K. (1923). Die Berechnug der Durchlassigkeit des Tones aus dem Verlauf der hydromechanischen Spannungserscheinungen. *Sitzungsber. Akad. Wiss.(Wien). Math.-Naturwiss. Kl., Abt. Iia*, *132*, 125–138.

Walker, R. L., Knepley, M. G., Aagaard, B. T., & Williams, C. A. (2023). Multiphysics modelling in PyLith: Poroelasticity. *Geophysical Journal International*, *235*(3), 2442–2475. https://doi.org/10.1093/gji/ggad370